J|A|C|S ARTICLES

Published on Web 12/22/2010

Sensitizing the Sensitizer: The Synthesis and Photophysical Study of Bodipy−Pt(II)(diimine)(dithiolate) Conjugates

Theodore Lazarides, Theresa M. McCormick, Kristina C. Wilson, Soohyun Lee, David W. McCamant,* and Richard Eisenberg*

Department of Chemistry, University of Rochester, Rochester, New York 14627, United States

Received August 5, 2010; E-mail: mccamant@chem.rochester.edu; eisenberg@chem.rochester.edu

Abstract: The dyads **3**, **4**, and **6**, combining the Bodipy chromophore with a Pt(bpy)(bdt) (bpy = 2,2′-bipyridine, bdt = 1,2-benzenedithiolate, **3** and **6**) or a Pt(bpy)(mnt) (mnt = maleonitriledithiolate, **4**) moiety, have been synthesized and studied by UV−vis steady-state absorption, transient absorption, and emission spectroscopies and cyclic voltammetry. Comparison of the absorption spectra and cyclic voltammograms of dyads **3**, **4**, and **6** and those of their model compounds **1a**, **2**, **5**, and **7** shows that the spectroscopic and electrochemical properties of the dyads are essentially the sum of their constituent chromophores, indicating negligible interaction of the constituent chromophores in the ground state. However, emission studies on **3** and **6** show a complete absence of both Bodipy-based fluorescence and the characteristic luminescence of the Pt(bpy)(bdt) unit. Dyad **4** shows a weak Pt(mnt)-based emission. Transient absorption studies show that excitation of the dyads into the Bodipy-based $^1\pi\pi^*$ excited state is followed by singlet energy transfer (SEnT) to the Pt(dithiolate)-based ^{1}MMLL′CT (mixed metal-ligand to ligand charge transfer) excited state ($\tau^{\mathbf{3}}_{\mathrm{SEnT}} = 0.6$ ps, $\tau^{\mathbf{4}}_{\mathrm{SEnT}} = 0.5$ ps, and $\tau^{\mathbf{6}}_{\mathrm{SEnT}} = 1.6$ ps), which undergoes rapid intersystem crossing to the ^{3}MMLL′CT state due to the heavy Pt(II) ion. The ^{3}MMLL′CT state is then depopulated by triplet energy transfer (TEnT) to the low-lying Bodipy-based $^3\pi\pi^*$ excited state ($\tau^{\mathbf{3}}_{\mathrm{TEnT}} = 8.2$ ps, $\tau^{\mathbf{4}}_{\mathrm{TEnT}} = 5$ ps, and $\tau^{\mathbf{6}}_{\mathrm{TEnT}} = 160$ ps). The transition assignments are supported by TD-DFT calculations. Both energy-transfer processes are shown to proceed via a Dexter electron exchange mechanism. The much longer time constants for dyad **6** relative to **3** are attributed to the significantly poorer coupling and resonance of charge-separated species that are intermediates in the electron exchange process.

Introduction

Multichromophoric species have enjoyed continuing interest in their photochemistry and photophysical properties due to their potential for applications in the development of synthetic systems for light harvesting and storage and in optoelectronic devices.[1−3] In this work, we describe new systems combining a Pt(II)(diimine)(dithiolate) complex and a boron dipyrrin (Bodipy) dye. Pt(II)(diimine)(dithiolate) complexes have been studied extensively due to their photoabsorption in the visible spectrum, which gives rise to long-lived charge-transfer excited states, leading to luminescence in the orange-red and near-infrared regions of the spectrum.[4−7] These excited states have been shown by Arakawa to be reductive enough to transfer electrons to nanocrystalline titanium dioxide, leading to the generation of photocurrent.[8,9] They are also capable of electron-transfer quenching, which can initiate a photocatalytic cycle for the production of hydrogen from water in the presence of a sacrificial donor.[10] However, despite the desirable redox properties of the Pt(II)(diimine)(dithiolate) excited states, their relatively modest molar absorptivities (maximum $\varepsilon \approx 10^4$ M^{-1} cm^{-1}) represent a drawback in their use for H_2 photogeneration.

In order to improve the light-harvesting potential of these chromophores, we describe herein studies in which the Pt(II)(diimine)(dithiolate) chromophore is connected to a strongly absorbing dye ($\varepsilon \approx 10^5$ M^{-1} cm^{-1}) in a dual-chromophore system that is constructed to sensitize the generation of the Pt-based charge-transfer excited state by efficient photoinduced energy transfer. The dye used in this study is a member of the Bodipy (boron−dipyrromethene) dyes that have been studied and used in numerous applications ranging from metal ion and gas sensing to protein labeling.[11−15] Bodipy dyes exhibit intense absorption and emission in the visible region corresponding to a $^1\pi\pi^*$ excited state, which lies higher in energy than the corresponding charge-transfer energy levels of a typical Pt(II)(diimine)(dithiolate) chromophore. By covalently linking the strongly absorbing Bodipy dye to the

(1) Ward, M. D. *Chem. Soc. Rev.* **1997**, *26*, 365–375.
(2) Ward, M. D. *Chem. Soc. Rev.* **1995**, *24*, 121–134.
(3) Balzani, V.; Bergamini, G.; Ceroni, P. *Coord. Chem. Rev.* **2008**, *252*, 2456–2469.
(4) Zuleta, J. A.; Burberry, M. S.; Eisenberg, R. *Coord. Chem. Rev.* **1990**, *97*, 47–64.
(5) Zuleta, J. A.; Bevilacqua, J. M.; Eisenberg, R. *Coord. Chem. Rev.* **1991**, *111*, 237–248.
(6) Paw, W.; Cummings, S. D.; Mansour, M. A.; Connick, W. B.; Geiger, D. K.; Eisenberg, R. *Coord. Chem. Rev.* **1998**, *171*, 125–150.
(7) Cummings, S. D.; Eisenberg, R. *J. Am. Chem. Soc.* **1996**, *118*, 1949–1960.
(8) Islam, A.; Sugihara, H.; Hara, K.; Singh, L. P.; Katoh, R.; Yanagida, M.; Takahashi, Y.; Murata, S.; Arakawa, H. *Inorg. Chem.* **2001**, *40*, 5371–5380.
(9) Geary, E. A. M.; Yellowlees, L. J.; Jack, L. A.; Oswald, I. D. H.; Parsons, S.; Hirata, N.; Durrant, J. R.; Robertson, N. *Inorg. Chem.* **2005**, *44*, 242–250.
(10) Zhang, J.; Du, P. W.; Schneider, J.; Jarosz, P.; Eisenberg, R. *J. Am. Chem. Soc.* **2007**, *129*, 7726.
(11) Ziessel, R.; Camerel, F.; Donnio, B. *Chem. Rec.* **2009**, *9*, 1–23.
(12) Ziessel, R.; Ulrich, G.; Harriman, A.; Alamiry, M. A. H.; Stewart, B.; Retailleau, P. *Chem.—Eur. J.* **2009**, *15*, 1359–1369.

 10.1021/ja1070366

Pt(II)(diimine)(dithiolate) complex, it was expected that energy transfer from the Bodipy to the mixed metal-ligand-to-ligand charge-transfer (MMLL′CT) state of the Pt complex would occur. Two complexes were synthesized, **3** and **6**, one with the Bodipy connected to the diimine, using ligand **1a**, and the other with a connection to the dithiolate **1b** (shown below). The photophysical properties were compared to those previously reported for Pt(II)-(diimine)(dithiolate) complexes and the model Pt(bpy)(bdt) complex **7**. Complexes **2** and **4** were synthesized to determine the effect of varying the Pt-based charge transfer excited state energy on the overall energy-transfer dynamics. By attaching the Bodipy moiety to the metal complex, emission was quenched in all the dyads, **2**−**6**. Transient absorption spectroscopy and time-dependent DFT calculations indicate a possible route to nonradiative decay through the $^3\pi\pi^*$ Bodipy state, and they also suggest a possible route for connecting strongly absorbing dyes to charge-transfer complexes such that electron injection into nanocrystalline titanium dioxide for photocurrent or for the photoreduction of hydrogen can be achieved.

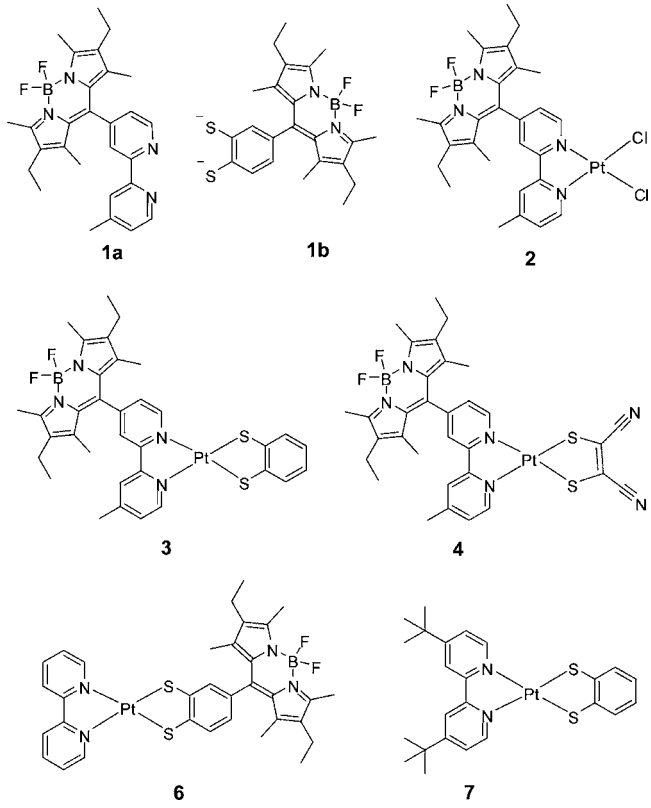

Experimental Section

Chemicals. 4-Formyl-4′-methyl-2,2′-bipyridine,[16] 2-oxobenzo[*d*][1,3]-dithiole-5-carbaldehyde,[17] *cis*-Pt(DMSO)$_2$Cl$_2$,[18] and Pt(dbbpy)Cl$_2$[19] were prepared according to published procedures. The synthesis of Bodipy dyes also followed published procedures, with modifications detailed below.[20] All other chemical precursors and solvents were obtained by commercial sources and were used as received.

Characterization. ^{1}H NMR and ^{13}C NMR spectra were recorded on a Bruker AMX-400 or Avance 400 spectrometer (400 MHz). Elemental analyses were provided by Desert Analytics (Tucson, AZ). Cyclic voltammetry experiments were conducted on a EG&G PAR 263 A potentiostat/galvanostat using a three-electrode single-cell compartment. All samples were degassed with nitrogen before sampling and blanketed with nitrogen during the run. A Pt working electrode, a Pt wire auxiliary electrode, and a saturated calomel reference electrode (SCE) were used. The scan rate was 150 mV/s. For all measurements, tetrabutylammonium hexafluorophosphate was used as the supporting electrolyte with ferrocene as an internal reference [ferrocenium/ferrocene (Fc^+/Fc) couple 0.46 V versus SCE in CH_2Cl_2[21]]. Absorption spectra were recorded using a Hitachi U2000 scanning spectrophotometer (200−1100 nm). Steady-state luminescence spectra were measured on a Spex Fluoromax-P fluorometer and corrected for instrument response.

X-ray Crystallography. A crystal was placed onto the tip of a 0.1 mm diameter glass capillary tube or fiber and mounted on a Bruker SMART APEX II CCD Platform diffractometer for data collection at 100.0(1) K. A preliminary set of cell constants and an orientation matrix were calculated from 124 reflections harvested from three sets of 20 frames. These initial sets of frames were oriented such that orthogonal wedges of reciprocal space were surveyed. The data collection was carried out using Mo Kα radiation (graphite monochromator) with a frame time of 30 s and a detector distance of 5.02 cm. A randomly oriented region of reciprocal space was surveyed: four major sections of frames were collected with 0.50° steps in ω at four different ϕ settings and a detector position of −33° in 2θ. The intensity data were corrected for absorption.[22] Final cell constants were calculated from the *xyz* centroids of 4034 strong reflections from the actual data collection after integration. The structure was solved using SHELXL-974 and refined using SHELXL-97.[23] All non-hydrogen atoms were refined with anisotropic displacement parameters. All hydrogen atoms were placed in ideal positions and refined as riding atoms with relative isotropic displacement parameters. A summary of crystallographic data for these three compounds is included in the Supporting Information as Table S1 and in CIF format. Selected bond lengths for complex **3** and the model complex **7** are included in Table 1 (below).

Transient Absorption. Femtosecond transient absorption measurements were performed with a regeneratively amplified titanium: sapphire laser producing 1.7 mJ, 100 fs duration pulses at 800 nm with a 1 kHz repetition rate. The 530, 600, or 615 nm pump pulse was produced by a home-built non-collinear phase-matched optical parametric amplifier and was temporally compressed and attenuated to 0.18 μJ/pulse at the sample.[24,25] Care was taken to limit the bandwidth of the pump pulse in order to eliminate problems associated with simultaneous excitation of both the Bodipy $^1\pi\pi^*$ and the Pt(bpy)(bdt) ^{1}MMLL′CT absorption bands. The probe continuum extended from 330 to 660 nm and was produced by focusing a small portion of the 800 nm pulse into a 2 mm thick CaF_2 crystal. The relative polarization of the pump and probe beams was 55°, to eliminate artifacts from molecular rotation. After the sample, the probe beam was collected, dispersed by a spectrograph (Acton 320 mm fl, 150 g/mm), and measured with a 1024 pixel diode array detector (Spectronic Devices). Each transient absorption spectrum is generated from 2000 laser pulses, in which the alternating pump-off and pump-on spectra are compared in 100 ms exposures to produce the transient

(13) Meallet-Renault, R.; Pansu, R.; Amigoni-Gerbier, S.; Larpent, C. *Chem. Commun.* **2004**, 2344–2345.
(14) Baruah, M.; Qin, W. W.; Vallee, R. A. L.; Beljonne, D.; Rohand, T.; Dehaen, W.; Boens, N. *Org. Lett.* **2005**, *7*, 4377–4380.
(15) Loudet, A.; Burgess, K. *Chem. Rev.* **2007**, *107*, 4891–4932.
(16) Strouse, G. F.; Schoonover, J. R.; Duesing, R.; Boyde, S.; Jones, W. E.; Meyer, T. J. *Inorg. Chem.* **1995**, *34*, 473–487.
(17) Ishikawa, Y.; Miyamoto, T.; Yoshida, A.; Kawada, Y.; Nakazaki, J.; Izuoka, A.; Sugawara, T. *Tetrahedron Lett.* **1999**, *40*, 8819–8822.
(18) Price, J. H.; Schramm, R. F.; Wayland, B. B.; Williams, An. *Inorg. Chem.* **1972**, *11*, 1280.
(19) Rendina, L. M.; Vittal, J. J.; Puddephatt, R. J. *Organometallics* **1995**, *14*, 1030–1038.
(20) Ulrich, G.; Ziessel, R. *J. Org. Chem.* **2004**, *69*, 2070–2083.
(21) Connelly, N. G.; Geiger, W. E. *Chem. Rev.* **1996**, *96*, 877–910.
(22) Blessing, R. *Acta Crystallogr.* **1995**, *A51*, 33–38.
(23) *SHELXTL*, Version 6.14; Bruker AXS: Madison, WI, 2000.
(24) Cerullo, G.; De Silvestri, S. *Rev. Sci. Instrum.* **2003**, *74*, 1–18.
(25) Megerle, U.; Pugliesi, I.; Schriever, C.; Sailer, C.; Riedle, E. *Appl. Phys. B* **2009**, *96*, 215–231.

absorption spectrum for a single pump−probe time delay. The time delay was controlled by optically delaying the pump pulse, and the time resolution was 60−150 fs, depending on wavelength. Any scattering from the pump pulse was removed manually after the experiment. Kinetics at individual probe wavelengths were fit to a convolution of the Gaussian instrument response with a sum of exponential decays, while allowing the $\Delta t = 0$ time delay to vary to compensate for chirp in the probe.

Samples were prepared in dichloromethane, degassed with nitrogen, and sealed in 1 mm path length cuvettes. The OD at the pump wavelength was in the range of 0.3−0.7, and UV−vis spectra before and after each experiment verified that no sample degradation occurred during the experiment. The sample was continuously translated to interrogate a new sample region with each pair of pump−probe pulses. For the 600 and 615 nm pump experiments, the large OD required for the ^{1}MMLL′CT absorption made the absorption at the Bodipy $^1\pi\pi^*$ around 530 nm completely opaque; hence, spectra are blank in that region.

Quantum Chemical Calculations. The geometric parameters from X-ray diffraction analysis were used as the starting point for the geometry optimization when available. The computational analogues **1a′**−**7′** are identical to **1a**−**7**, except that the peripheral ethyl groups on Bodipy and the *tert*-butyl groups on **7** were replaced with methyl groups to decrease the computational expense. The Gaussian suite of programs (Gaussian 09)[26] was used for the restricted density functional theory calculations at the CAM-B3LYP[27] (Handy and co-workers' long-range corrected version of B3LYP using the Coulomb-attenuating method) level of theory, using LAN2DZ basis set on the Pt atoms and 6-31+G(d) basis set for the rest. TD-DFT calculations using the optimized geometrical parameters and the same basis set were performed. The parameters for the optimized geometries and full list of excited states are included in the Supporting Information.

Synthesis of the Ligands and Complexes. 5-(1,3,5,7-Tetraethyl-2,6-diethyl-4,4-difluoro-4-bora-3a,4a-diaza-*s*-indaceno)-5′-methyl-2,2′-bipyridine (1a). 5-Formyl-5′-methyl-2,2′-bipyridine (0.50 g, 2.5 mmol), 2,4-dimethyl-3-ethylpyrrole (0.6 mL, 5.2 mmol), and one drop of CF_3COOH were dissolved in anhydrous and deoxygenated CH_2Cl_2 (50 mL) and then stirred at room temperature under N_2 for 5 days. DDQ (0.63 g, 2.8 mmol) was then added to the reaction as a solid, and the system was stirred for ∼1 h. Triethylamine (1 mL) was added, followed by dropwise addition of $BF_3{\cdot}OEt_2$ (1 mL), and was stirred for ∼12 h. The reaction mixture was washed with 20 mL of saturated aqueous $NaHCO_3$. The aqueous layer was further extracted with 20 mL of CH_2Cl_2. The combined organic layers were dried with $MgSO_4$, filtered, and solvent evaporated. The product was purified by column chromatography on silica gel and eluted with CH_2Cl_2/MeOH 95:5 to afford the desired product as a red powder. Yield 0.30 g (25%). ^{1}H NMR ($CDCl_3$, 400 MHz): δ 8.80 (d, 1H, $J = 4$ Hz, bpy aromatic), 8.52 (d, 1H, $J = 4$ Hz, bpy aromatic), 8.48 (br s, H, bpy aromatic), 8.32 (br s, 1H, bpy aromatic), 7.31 (dd, 1H, $J_1 = 4$ Hz, $J_2 = 2.8$ Hz, bpy aromatic), 7.16 (d, 1H, $J = 4$ Hz, bpy aromatic), 2.54 (s, 6H, CH_3 on Bodipy closest to N), 2.47 (s, 3H, CH_3 on bpy), 2.29 (q, 4H, $J = 6$ Hz, CH_2 of ethyl groups), 1.37 (s, 6H, CH_3 on Bodipy), 0.99 (t, 6H, $J = 6$ Hz, CH_3 of ethyl groups). ^{13}C NMR ($CDCl_3$, MHz): δ 157.50, 154.99, 154.56, 149.73, 149.24, 148.26, 145.36, 137.90, 136.67, 133.23, 129.80, 125.19, 123.43, 121.93, 121.23, 21.21, 17.05, 14.57, 12.58, 12.19. ESI-MS (*m*/*z*): 473 $[M+H]^+$. Anal. Calcd for $C_{28}H_{31}BF_2N_4$: C, 71.19; H, 6.61; N, 11.86. Found: C, 70.98; H, 6.89; N, 11.74.

Pt(1a)Cl$_2$ (2). The ligand **1a** (0.10 g, 0.21 mmol), *cis*-[$(DMSO)_2PtCl_2$] (0.089 g, 0.21 mmol), and toluene (20 mL) were stirred at 80 °C under an atmosphere of nitrogen for 5 h, during which time a red precipitate appeared. The system was then cooled to room temperature, and the product was collected by filtration and washed with diethyl ether (2 × 3 mL). Yield 0.13 g (84%). ^{1}H NMR ($CDCl_3$, 400 MHz): δ 10.00 (d, 1H, $J = 6$ Hz, bpy aromatic), 9.65 (d, 1H, $J = 6$ Hz, bpy aromatic), 8.00 (br s, 1H, bpy aromatic), 7.81 (br s, 1H, bpy aromatic), 7.60 (dd, 1H, $J_1 = 6$ Hz, $J_2 = 1.5$ Hz, bpy aromatic), 7.45 (d, 1H, $J = 6$ Hz, bpy aromatic), 2.54 (s, 6H, CH_3 on Bodipy closest to N), 2.52 (s, 3H, CH_3 on bpy), 2.29 (q, 4H, $J = 7.5$ Hz, CH_2 of ethyl groups), 1.40 (s, 6H, CH_3 on Bodipy), 0.99 (t, 6H, $J = 7.5$ Hz, CH_3 of ethyl groups). ^{13}C NMR ($CDCl_3$, MHz): δ 158.13, 156.50, 155.91, 152.36, 150.44, 149.66, 148.26, 137.27, 134.51, 133.17, 129.14, 128.58, 127.63, 123.85, 122.95, 22.02, 17.22, 14.65, 13.10, 12.87. ESI-MS (*m*/*z*): 738 $[M]^+$. Anal. Calcd for $C_{28}H_{31}BCl_2F_2N_4Pt$: C, 45.55; H, 4.23; N, 7.59. Found: C, 45.12; H, 4.62; N, 7.71.

Pt(1a)(benzenedithiolate) (3). Complex **2** (0.050 g, 0.068 mmol) was dissolved in 10 mL of deaerated methanol, and 1,2-benzenedithiol (bdt) (0.010 g, 0.070 mmol) was added, followed by potassium *tert*-butoxide (0.016 g, 0.14 mmol). The red solution immediately darkened, and a purple precipitate appeared. The suspension was further stirred at room temperature under an atmosphere of nitrogen for 2 h; the solid was collected by filtration. The crude product was purified by column chromatography on silica gel using CH_2Cl_2/hexanes 1:1 as the eluent, affording the desired product as a dark purple crystalline solid after solvent evaporation. Yield 0.030 g (53%). ^{1}H NMR (CD_2Cl_2, 400 MHz): δ 9.49 (d, 1H, $J = 6$ Hz, bpy aromatic), 9.20 (d, 1H, $J = 6$ Hz, bpy aromatic), 8.11 (br s, 1H, bpy aromatic), 7.88 (br s, 1H, bpy aromatic), 7.58 (dd, 1H, $J_1 = 6$ Hz, $J_2 = 1.6$ Hz, bpy aromatic), 7.43 (d, 1H, $J = 6$ Hz, bpy aromatic), 7.37 (m, 2H, dithiolate aromatic), 6.78 (m, 2H, dithiolate aromatic), 2.54 (s, 6H, CH_3 on Bodipy), 2.47 (s, 3H, CH_3 on bpy), 2.36 (q, 4H, $J = 7.6$ Hz, CH_2 of ethyl groups), 1.48 (s, 6H, CH_3 on Bodipy), 1.01 (t, 6H, $J = 7.6$ Hz, CH_3 of ethyl groups). ^{13}C NMR (CD_2Cl_2, MHz): δ 156.68, 155.84, 154.67, 151.02, 149.41, 148.41, 146.58, 142.38, 137.64, 134.21, 133.96, 129.08, 128.96, 127.98, 124.07, 123.33, 121.83, 21.53, 16.95, 14.26, 12.75, 12.46. ESI-MS (*m*/*z*): 808 $[M+H]^+$. Anal. Calcd for $C_{34}H_{35}BF_2N_4PtS_2$: C, 50.56; H, 4.37; N, 6.94. Found: C, 50.24; H, 4.70; N, 7.20.

Pt(1a)(maleonitriledithiolate) (4). Complex **2** (0.050 g, 0.068 mmol) was dissolved in 10 mL of deaerated methanol, and disodium maleonitriledithiolate (Na_2mnt) (0.013 g, 0.070 mmol) was added. The red solution immediately darkened, and a red-purple precipitate appeared. The suspension was further stirred at room temperature under an atmosphere of nitrogen for 2 h, and the solvent was removed by evaporation. The crude product was purified by column chromatography on silica gel using CH_2Cl_2 as the eluent. The main dark red band was collected, and the solvent was removed, affording the desired product as a dark red crystalline solid. Yield 0.020 g (36%). ^{1}H NMR (CD_2Cl_2, 400 MHz): δ 9.22 (d, 1H, $J = 5.1$ Hz, bpy aromatic), 8.96 (d, 1H, $J = 5.1$ Hz, bpy aromatic), 8.18 (br s, 1H, bpy aromatic), 7.94 (br s, 1H, bpy aromatic), 7.68 (dd, 1H, $J_1 = 5.1$ Hz, $J_2 = 1.2$ Hz, bpy aromatic), 7.50 (d, 1H, $J = 5.1$ Hz, bpy aromatic), 2.56 (s, 6H, CH_3 on Bodipy), 2.43 (s, 3H, CH_3 on bpy), 2.35 (q, 4H, $J = 6.0$ Hz, CH_2 of ethyl groups), 1.44 (s, 6H, CH_3 on Bodipy), 1.01 (t, 6H, $J = 6.0$ Hz, CH_3 of ethyl groups). ^{13}C NMR (CD_2Cl_2, MHz): δ 156.69, 156.23, 149.55, 148.65, 145.51, 137.35, 134.59, 132.97, 132.63, 129.53, 129.03, 128.57, 124.52, 123.83, 121.15, 117.89, 116.16, 21.63, 16.95, 14.24, 12.78, 12.49. ESI-MS (*m*/*z*): 808 $[M+H]^+$. Anal. Calcd for $C_{32}H_{31}BF_2N_6PtS_2$: C, 47.59; H, 3.87; N, 10.41. Found: C, 47.28; H, 3.98; N, 10.15.

2-Oxobenzo[*d*][1,3]dithiole-5-(1,3,5,7-tetramethyl-2,6-diethyl-(4,4-difluoro-4-bora-3a,4a-diaza-*s*-indacene)) (5). In anhydrous and deoxygenated CH_2Cl_2 (30 mL), 2-oxobenzo[*d*][1,3]dithiole-5-carbaldehyde (0.300 g, 1.53 mmol), 2,4-dimethyl-3-ethylpyrrole (0.414 g, 3.40 mmol), and one drop of CF_3COOH were dissolved. The resulting solution was stirred at room temperature under an atmosphere of nitrogen for 5 days. DDQ (0.347 g, 1.53 mmol) was added to the reaction, and the system was stirred for ∼1 h. Triethylamine (0.5 mL) of was then added to the system, followed by dropwise addition of $BF{\cdot}OEt_2$ (0.5 mL). The solution was stirred

(26) Frisch, M. J.; et al. *Gaussian 09*; Gaussian, Inc.: Wallingford, CT, 2009.
(27) Yanai, T.; Tew, D.; Handy, N. *Chem. Phys. Lett.* **2004**, *393*, 51–57.

Scheme 1. Synthesis of the Compounds Discussed in This Paper

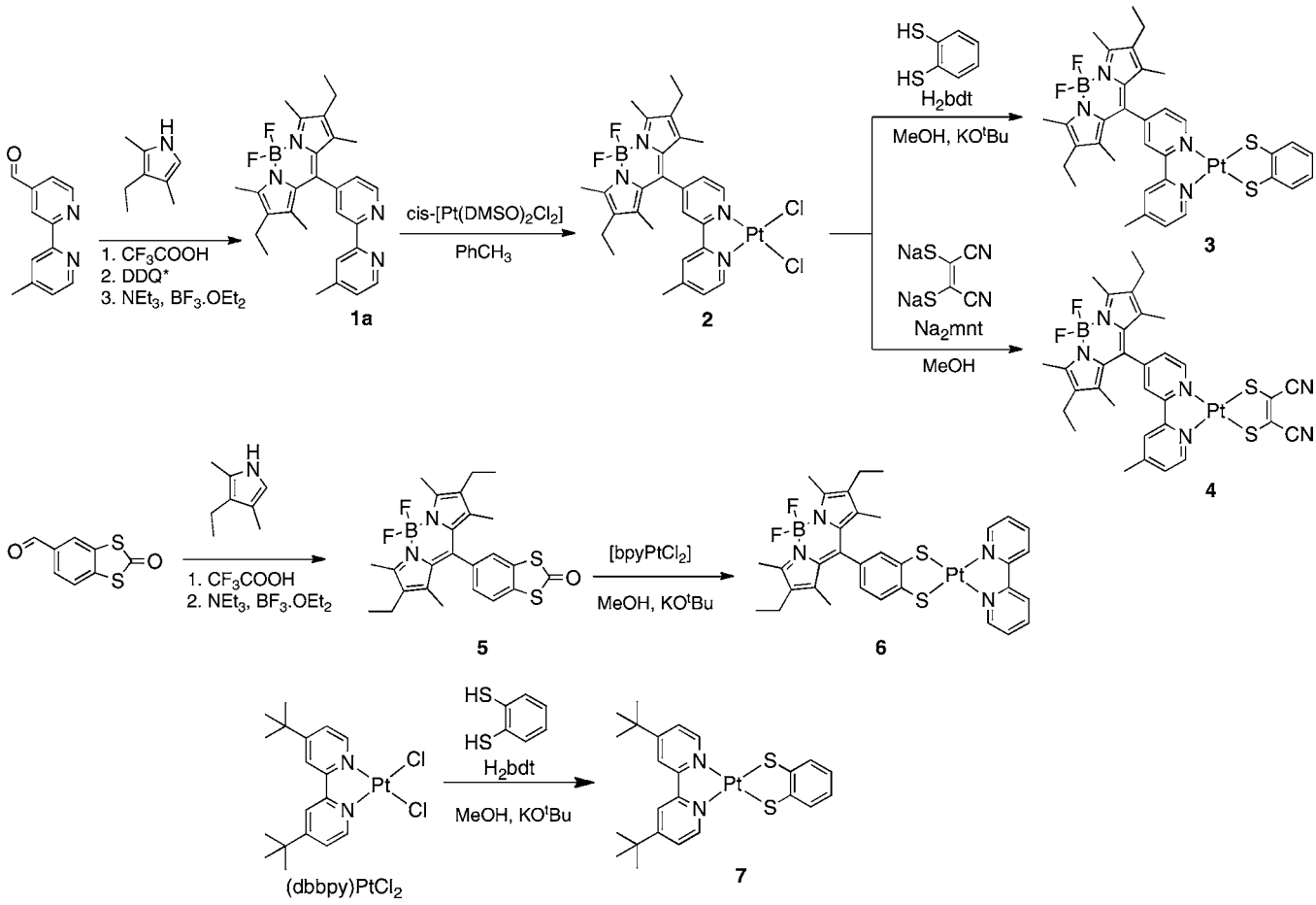

for 12 h and then washed with 20 mL of saturated aqueous $NaHCO_3$. The organic layer was collected, and the aqueous layer was further extracted with 20 mL of CH_2Cl_2. The combined organic layers were dried with $MgSO_4$, filtered, and evaporated. The crude product was purified by column chromatography on silica gel, eluting with CH_2Cl_2, to afford the desired product as a red powder. Yield 0.120 g (17%). ^{1}H NMR ($CDCl_3$, 400 MHz): δ 7.62 (d, 1H, $J = 6.4$ Hz, dithiolene aromatic), 7.45 (d, 1H, $J = 1.6$ Hz, dithiolene aromatic), 7.28 (dd, 1H, $J_1 = 6.4$, $J_2 = 1.6$, dithiolene aromatic), 2.54 (s, 6H, CH_3 on Bodipy), 2.31 (q, 4H, $J = 6.0$ Hz, CH_2 of ethyl groups), 1.36 (s, 6H, CH_3 on Bodipy), 0.99 (t, 6H, $J = 6.0$ Hz, CH_3 of ethyl groups). ^{13}C NMR ($CDCl_3$, MHz): δ 189.08, 154.63, 137.86, 137.24, 134.98, 133.63, 133.29, 130.60, 127.26, 123.56, 122.93, 17.07, 14.57, 12.57, 12.18. EI-MS (*m*/*z*): 470 $[M]^+$, 455 $[M-CH_3]^+$, 427 $[M-CH_3-CO]^+$. Anal. Calcd for $C_{24}H_{25}BF_2N_2OS_2$: C, 61.28; H, 5.36; N, 5.96. Found: C, 60.89; H, 5.64; N, 5.62.

Pt(1b)(2,2′-bipyridine) (6). Ligand precursor **5** (0.050 g, 0.11 mmol) was suspended in 10 mL of deaerated methanol, and potassium *tert*-butoxide (0.024 g, 0.22 mmol) was added. The system was stirred for 15 min at room temperature under an atmosphere of N_2 before [bpyPtCl$_2$] (0.046 g, 0.11 mmol) was added. The suspension was further stirred for 48 h, during which time a purple precipitate formed. The solvent was removed, and the crude product was purified by column chromatography on silica gel using CH_2Cl_2/hexanes 1:1 as eluent. The main purple band was collected, and the solvent was removed, affording the desired product as a red-purple solid. Yield 0.030 g (34%). ^{1}H NMR (CD_2Cl_2, 400 MHz): δ 9.32 (dd, 2H, $J_1 = 14.1$ Hz, $J_2 = 5.2$ Hz, bpy aromatic), 8.15 (m, 4H, bpy aromatic), 7.58 (m, 2H, bpy aromatic), 7.48 (d, 1H, $J = 6.5$ Hz, dithiolate aromatic), 7.24 (d, 1H, $J = 1.2$ Hz, dithiolate aromatic), 6.69 (dd, 1H, $J_1 = 6.5$ Hz, $J_2 = 1.2$ Hz, dithiolate aromatic), 2.50 (s, 6H, CH_3 on Bodipy), 2.34 (q, 4H, $J = 6.0$ Hz, CH_2 of ethyl groups), 1.45 (s, 6H, CH_3 on Bodipy), 1.01 (t, 6H, $J = 6.0$ Hz, CH_3 of ethyl groups). ^{13}C NMR (CD_2Cl_2, MHz): δ 155.7, 152.9, 148.9, 143.7, 141.5, 138.9, 138.4, 132.5, 131.0, 128.8, 128.4, 127.8, 127.3, 123.1, 121.6, 16.9, 14.4, 12.2, 11.9. EI-MS (*m*/*z*): 794 $[M+H]^+$, 774 $[M-F]^+$. Anal. Calcd for $C_{33}H_{33}BF_2N_4PtS_2$: C, 49.94; H, 4.19; N, 7.06. Found: C, 49.62; H, 4.38; N, 6.79.

Pt(5,5′-*tert*-butyl-2,2′-bipyridine)(benzenedithiolate) (7). (dbbpy)-$PtCl_2$ (0.10 g, 0.19 mmol) was suspended in 10 mL of deaerated methanol, and 1,2-benzenedithiol (bdt) (0.027 g, 0.19 mmol) was added, followed by potassium *tert*-butoxide (0.045 g, 0.4 mmol). The suspension gradually darkened, and a purple precipitate appeared. The suspension was further stirred at room temperature under an atmosphere of nitrogen for 6 h, and the solid was collected by filtration. The crude product was purified by column chromatography on silica gel using CH_2Cl_2/hexanes 1:1 as eluent. The main purple band was collected, and the solvent was removed, affording the desired product as a purple crystalline solid. Yield 0.096 g (84%). ^{1}H NMR ($CDCl_3$, 400 MHz): δ 9.15 (d, 2H, $J = 6.0$ Hz, bpy aromatic), 7.90 (d, 2H, $J = 1.2$ Hz, bpy aromatic), 7.44 (m, 4H, bpy and dithiolate aromatic), 6.80 (m, 2H, dithiolate aromatic), 1.47 (s, 18H, *tert*-butyl groups). ^{13}C NMR (CD_2Cl_2, MHz): δ 162.7, 155.6, 148.4, 142.2, 128.2, 124.7, 121.8, 119.4, 35.7, 30.2. EI-MS (*m*/*z*): 604 $[M+H]^+$. Anal. Calcd for $C_{24}H_{28}N_2PtS_2$: C, 47.75; H, 4.67; N, 4.64. Found: C, 47.42; H, 4.48; N, 4.37.

Results

Syntheses of Ligands and Complexes. Scheme 1 shows the syntheses of the ligands and complexes discussed in this paper. The specific Bodipy derivatives **1a** and **5** (the isolated precursor

to **1b**) were prepared, beginning with the initial acid-catalyzed reaction of the corresponding aldehydes with 1,3-dimethyl-2-ethylpyrrole to yield the initial dipyrrole derivatives. These dipyrrole compounds were then oxidized by 2,3-dichloro-5,6-dicyanobenzoquinone (DDQ) to give the corresponding unsaturated dipyrrins that were then treated with boron trifluoride in the presence of base to yield the desired Bodipy-derivatized ligand **1a** and the dithiolate precursor **5**.[7,20] The Pt(II) dichloride complex **2** was prepared by reaction of **1a** with *cis*-$Pt(DMSO)_2Cl_2$ and was then easily isolated as a precipitate from the reaction mixture. Subsequent reaction of **2** with 1,2-benzenedithiol (bdt) in the presence of base or the sodium salt of maleonitriledithiolate (Na_2mnt) led to the formation of the dual chromophore Pt(II)(diimine)(dithiolate)−Bodipy conjugates **3** and **4**, respectively.

In a different reaction sequence, compound **5** was reacted with K(O*t*Bu) in order to unmask and deprotect the dithiolate ligand **1b** *in situ*,[28] after which the Bodipy-derivatized benzenedithiolate was reacted with $Pt(bpy)Cl_2$ to give complex **6**. The model Pt(II)(diimine)(dithiolate) compound **7** was prepared from the corresponding diimine dichloride complex using modified literature methods for the synthesis of analogous complexes.[7] The new compounds **1a**, **2**, **3**, **4**, **5**, **6**, and **7** were characterized on the basis of their ^{1}H and ^{13}C NMR spectra, ESI or EI mass spectra, and elemental analyses.

Structural Characterization of 1a, 3, and 7. Compounds **1a**, **3**, and **7** were structurally characterized by X-ray crystallography (Figure 1). A collection of the most important bond lengths and angles for **3** and **7** can be seen in Table 1. Complete structural parameters for each species and a summary of crystallographic data are presented in Supporting Information as Tables S1 and S2 and in a separate CIF. In the crystal structures of **1a** and **3**, the Bodipy moieties exhibit the expected planar arrangement of the dipyrrin group and nearly tetrahedral geometry about the boron atom. The B−N and B−F distances (∼1.55 and 1.39 Å, respectively) correlate well to those found in other Bodipy derivatives.[29−31] In **1a** and **3**, the bpy and Pt(bpy)(bdt) planes are nearly perpendicular to those of the corresponding Bodipy moieties (torsion angles ∼89° for **3** and ∼78° for **1a**). Both **1a** and **3** are "locked" in this conformation due to the steric hindrance induced by the methyl substituents of the dipyrrin units with the attached pyridyl ring. The Pt(bpy)(bdt) moieties in **3** and **7** show the expected distorted square planar geometry about the Pt atom. The main source of distortion from square planar coordination is the small bite angle of the bpy ligand (∼80°). The average Pt−N and Pt−S distances are ca. 2.05 and 2.25 Å, respectively, and are well within the expected range for Pt(bpy)(bdt) complexes.[32]

Absorption and Emission Spectra. The UV−vis absorption and emission spectra of the compounds described in this paper are summarized in Figure 2 and Table 2. The absorption spectra of ligands **1a** and **5** are dominated by the intense bands at 529 and 527 nm, respectively, having molar extinction coefficients ε in the range of 70 000 M^{-1} cm^{-1}. These absorption bands are due to the lowest energy spin-allowed $\pi\pi^*$ transitions of the Bodipy units.[33] In addition, **1a** and **5** show absorption bands of lower intensity in the 280−380 nm region, attributed to higher energy $\pi\pi^*$ transitions of the Bodipy moiety, bipyridine, or the

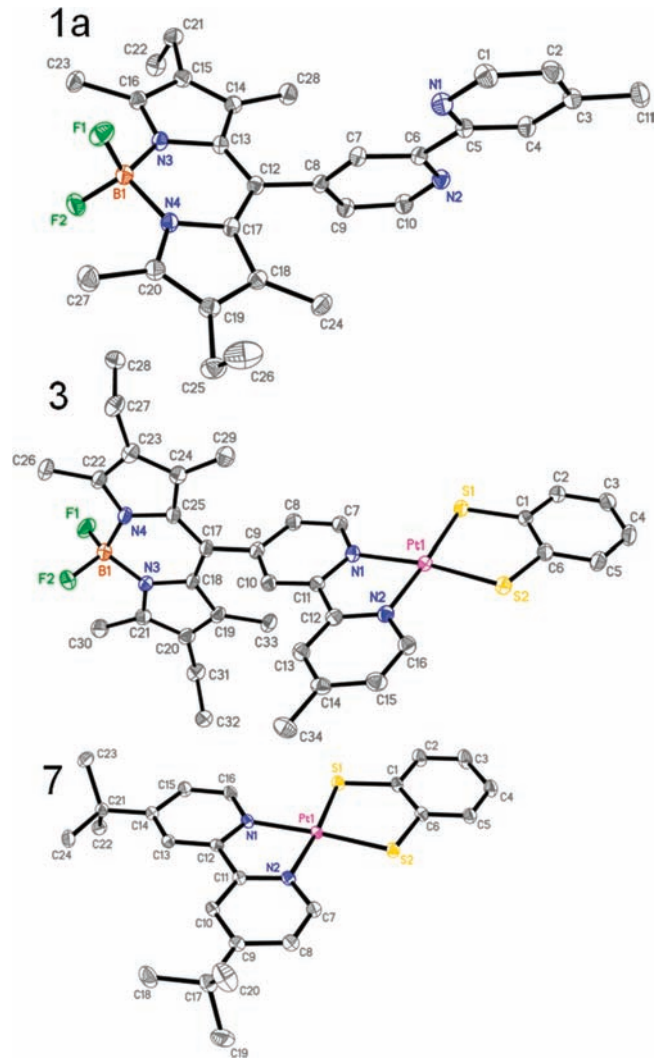

Figure 1. Molecular structure of **1a**, **3**, and **7** with thermal ellipsoids at the 50% probability level. Atom numbering schemes are shown; the hydrogen atoms are omitted for clarity. In **3**, the CH_2Cl_2 molecule of crystallization is omitted for clarity.

Table 1. Selected Bond Lengths (Å) and Angles (°) for **3** and **7**

	3	**7**
B1−F1	1.390(3)	
B1−F2	1.388(3)	
B1−N3	1.549(4)	
B1−N4	1.544(4)	
N3−C21	1.342(3)	
N3−C18	1.399(3)	
N4−C22	1.351(3)	
N4−C25	1.402(3)	
Pt1−N1	2.058(2)	2.039(2)
Pt1−N2	2.052(2)	2.047(2)
Pt1−S1	2.2574(6)	2.2507(6)
Pt1−S2	2.2425(6)	2.2531(6)
S1−C1	1.768(2)	1.752(2)
S2−C6	1.750(2)	1.752(2)
S1−Pt1−S2	88.82(2)	89.24(2)
N1−Pt1−N2	79.03(8)	78.96(7)
N1−Pt1−S1	97.96(6)	95.47(5)
N2−Pt1−S2	94.27(6)	96.34(5)

(28) Nomura, M.; Fourmigue, M. *Inorg. Chem.* **2008**, *47*, 1301–1312.
(29) Broring, M.; Kruger, R.; Link, S.; Kleeberg, C.; Kohler, S.; Xie, X.; Ventura, B.; Flamigni, L. *Chem.—Eur. J.* **2008**, *14*, 2976–2983.
(30) Bandichhor, R.; Thivierge, C.; Bhuvanesh, N. S. P.; Burgess, K. *Acta. Crystallogr. E* **2006**, *62*, O4310–O4311.
(31) Shen, Z.; Rohr, H.; Rurack, K.; Uno, H.; Spieles, M.; Schulz, B.; Reck, G.; Ono, N. *Chem.—Eur. J.* **2004**, *10*, 4853–4871.
(32) Connick, W. B.; Gray, H. B. *J. Am. Chem. Soc.* **1997**, *119*, 11620–11627.

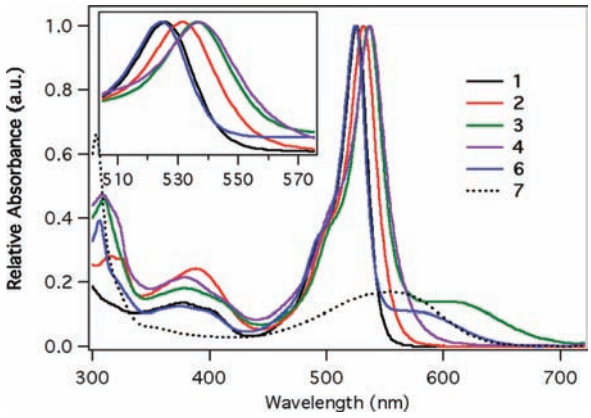

Figure 2. UV−vis absorption spectra of compounds **1a**, **2**, **3**, **4**, **6**, and **7** in dichloromethane. Spectra containing Bodipy have been normalized to give a maximum absorbance of **1**. The spectrum of **7**, the Pt(bpy)(bdt) chromophore, has been scaled to make its intensity comparable to the other MMLL′CT absorption bands at ∼600 nm. The inset shows an expanded region around the 530 nm Bodipy $\pi\pi^*$ absorption band.

Table 2. Absorption and Emission Data in Dichloromethane at Room Temperature

	absorption	emission	
compd	λ_{max}, nm (ε, M^{-1} cm^{-1})	λ_{max}, nm	Φ^a
1a	281 (20400), 378 (8300), 529 (70700)	535	0.57
2	279 (26000), 316 (14300), 393 (12300), 537 (53000)	590	0.33
3	309 (27300), 380 (10200), 536 (60200), 597[b] (8300)	−	0
4	289 (23900), 309 (24800), 378 (11200), 538 (52200)	594	0.004
5	278 (19600), 384 (9200), 527 (83400)	532	0.61
6	264 (63100), 294 (39600), 305 (43600), 374 (13800), 524 (107700), 568[b] (11800)	−	0
7	302 (30270), 560 (7800)	695	0.096

[a] Corrected emission spectra were used with Rhodamine B in water as a standard. [b] Center wavelengths of the long-wavelength shoulders in **3** and **6** were determined by fitting the spectrum to a sum of Gaussians.

benzenedithiolate part (for **5**) of the molecule.[33] The absorption spectra of the metal complex−Bodipy conjugates **3**, **4**, and **6** are essentially the sums of those of their constituent chromophores.[33,34] The most interesting feature observed in the absorption spectra of **3** and **6** (see Figure 2) is a shoulder on the low-energy side of the intense Bodipy absorption bands (at 600 and 572 nm, respectively), which is attributed, after comparison with the spectrum of model compound **7**, to the singlet electronic transition from an orbital of mixed dithiolate−Pt character to one centered on the bipyridine ligand (a mixed metal/ligand-to-ligand′ charge transfer, or MMLL′CT).[34,35] This assignment is further supported by the observation that these shoulders shift to higher energies as the solvent polarity is increased (a blue shift of ∼10 nm when the solvent is changed to CH_2Cl_2/MeCN 1:1). This solvatochromism is a characteristic of the Pt(diimine)(dithiolate) complexes.[5,34] A shoulder like the ones described above is *not* seen in the absorption spectra of **2** and **4** because the charge transfer to diimine transitions of the $Pt(bpy)Cl_2$ and Pt(bpy)(mnt) complexes are shifted to higher energies relative to their bdt analogues[34] and thus are obscured by the strong Bodipy absorptions at similar energies.

Table 3. Summary of Oxidation and Reduction Potentials from Cyclic Voltammograms[a]

	$E_{1/2}$, V vs SCE	
compd	ox	red
1a	1.04	−1.30
2	1.00	−1.12
3	0.61 (irrev), 1.09	−1.08
4	1.06, 1.15	−1.03
5	1.04	−1.33
6	0.55 (irrev), 0.95	−1.49
7	0.56 (irrev)	−1.40

[a] Redox potentials were determined by cyclic voltammetry in dry CH_2Cl_2 containing 0.1 M of tetrabutylammonium hexafluorophosphate as a supporting electrolyte and a solute concentration of $1-1.5 \times 10^{-3}$ M. A saturated calomel electrode (SCE) was used as reference. Under these conditions, the reversible oxidation of ferrocene was $E_{1/2Fc} = +0.46$ V. All solutions were deoxygenated by purging with dry nitrogen prior to measurement.

The luminescence properties of the Bodipy−Pt(diimine)-(dithiolate) conjugates and their model compounds were studied in dichloromethane under ambient conditions. Emission maxima and quantum yields for the luminescent species are collected in Table 2. The Bodipy-derivatized diimine ligand **1a** and dithiolate precursor **5** show the intense fluorescence of a Bodipy dye at 535 and 532 nm, respectively, while the model Pt(diimine)(dithiolate) compound **7** exhibits the expected MMLL′CT-based luminescence at 690 nm. In contrast to their constituent chromophores, dyads **3** and **6** do not exhibit emission at room temperature or 77 K. Quenching of the Bodipy $^1\pi\pi^*$ state emission of these conjugates can be explained by efficient energy transfer to the lower-lying ^{1}MMLL′CT excited state, while quenching of the Pt(dbbpy)(bdt) part of the dyad may result from back energy transfer after intersystem crossing (ISC) to the $^3\pi\pi^*$ excited state of coordinated Bodipy. Support for this idea comes from the related work by Ziessel and Campagna,[36] in which complete emission quenching was observed in dyads containing Bodipy and either the $[Ru(bpy)_3]^{2+}$ or $[Ru(terpy)_2]^{2+}$ charge-transfer chromophore. The absence of MLCT emission from those systems was attributed to more rapid and efficient energy transfer from the ^{3}MLCT state to the $^3\pi\pi^*$ excited state of the Bodipy moiety.[36] A similar deactivation mechanism occurs for dyads **3** and **6**. For the Bodipy−$PtCl_2$ dyad **2** and the Bodipy−Pt(mnt) dyad **4**, emissions much weaker than those of their parent ligands are observed at 590 and 594 nm, respectively. It is worth noting that the chloride complex **2** has a much stronger emission than **4** but still much weaker than that of the parent ligand. These emission bands are attributed to red-shifted fluorescence from the Bodipy unit due the electronic influence of the bpy-coordinated Pt(II) ion. More detailed discussion on the formation and dynamic behavior of the excited states in the Bodipy−Pt(diimine)(dithiolate) conjugates is presented below in the section dealing with transient absorption studies.

Electrochemical Studies. Dyads **3**, **4**, and **6** and model compounds **1a**, **2**, **5** and **7** were studied by cyclic voltammetry, and their electrochemical data are collected in Table 3. All potentials are reported vs SCE. The cyclic voltammograms of the Bodipy-derivatized dichloride complex **2** and its dithiolate derivative **3** are shown in Figure 3. Based on comparison of

(33) Karolin, J.; Johansson, L. B. A.; Strandberg, L.; Ny, T. *J. Am. Chem. Soc.* **1994**, *116*, 7801–7806.
(34) Zuleta, J. A.; Bevilacqua, J. M.; Proserpio, D. M.; Harvey, P. D.; Eisenberg, R. *Inorg. Chem.* **1992**, *31*, 2396–2404.
(35) Adams, C. J.; Fey, N.; Parfitt, M.; Pope, S. J. A.; Weinstein, J. A. *Dalton Trans.* **2007**, 4446–4456.
(36) Galletta, M.; Puntoriero, F.; Campagna, S.; Chiorboli, C.; Quesada, M.; Goeb, S.; Ziessel, R. *J. Phys. Chem. A* **2006**, *110*, 4348–4358.

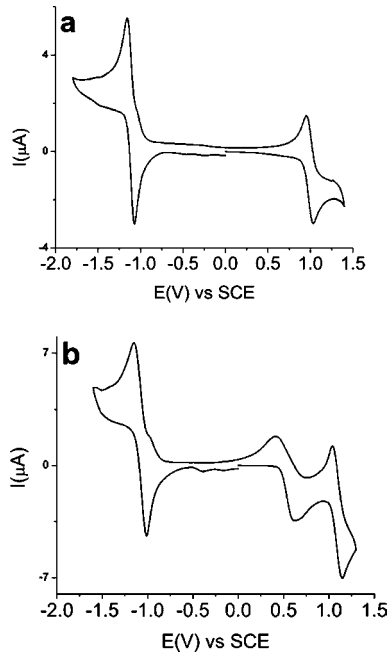

Figure 3. Cyclic voltammograms of **2** (a) and **3** (b) in CH_2Cl_2 using tetrabutylammonium hexafluorophosphate as supporting electrolyte with a scan rate of 150 mV/s.

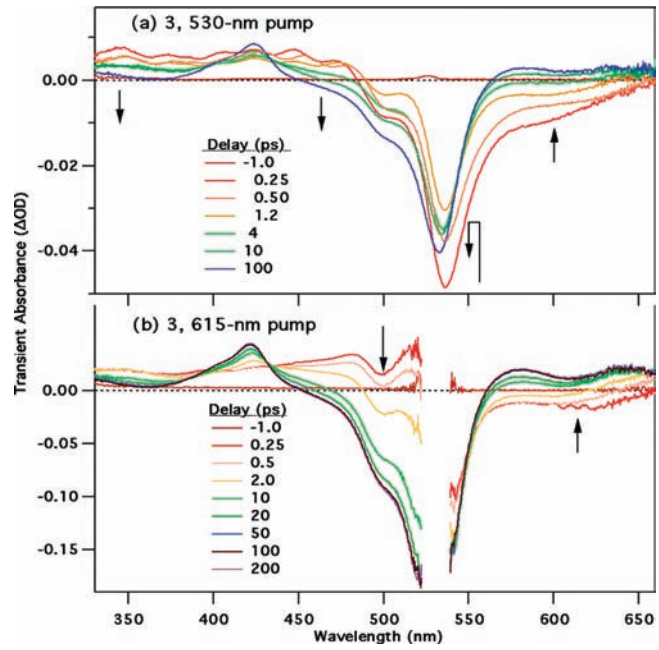

Figure 4. Femtosecond transient absorption spectra for **3** obtained with a 530 nm pump pulse (a) and a 615 nm pump pulse (b). The 530 nm excitation directly excites the $^1\pi\pi^*$ absorption band of the Bodipy moiety, whereas the 615 nm excitation excites the lower-energy MMLL′CT absorption centered on the Pt(bpy)(bdt) chromophore. In (b), the sample was opaque around 530 nm, so that region has been left blank. In each set of spectra the bleach of the Bodipy-based $^1\pi\pi^*$ band at 530 nm and the growth of the $^3\pi\pi^*$ absorption band at 425 nm is apparent.

the results with the CVs of the Bodipy-derivatized bipyridyl ligand **1a** and the Bodipy-linked benzenedithiolate precursor **5** and on electrochemical data reported in the literature,[36−38] the reversible processes occurring in the range between ca. 1.0 and 1.1 V vs SCE are attributed to the oxidation of the Bodipy unit to form the corresponding radical cation. In addition to the Bodipy-based oxidations, the dye−complex conjugates **3** and **6** show irreversible processes with peaks at 0.61 and 0.55 V, respectively, that correlate well with a peak in the CV of the model Pt(diimine)(dithiolate) complex **7**. These irreversible oxidations are therefore assigned to the Pt(bpy)(dithiolate) part of the conjugate.[34,35,39] Complex **4** shows two closely spaced, reversible oxidation processes at 1.06 and 1.15 V. These, with similar reasoning, are assigned to the Bodipy and Pt(mnt) moieties, respectively. Pt(diimine)(mnt) complexes such as **5** are known to show irreversible oxidations at higher potentials compared to their bdt counterparts such as **3**.[35]

The reversible reductions observed in the cyclic voltammograms of dyads **2**, **3**, and **4** are shifted to less negative potentials by ca. 0.2 V when compared to the reversible Bodipy-based reduction[36−38] at −1.30 V shown by the Bodipy-derivatized bpy ligand **1a**. In complexes **2**, **3**, and **4**, the reductions around −1.1 V are due to the bpy groups which are rendered better electron acceptors as a result of the electron-withdrawing effect of the Pt(II) ion. This assignment is consistent with what was observed by Ziessel et al. in Bodipy chromophores containing vacant bpy sites upon complexation with $[Ru(bpy)_2]^{2+}$.[36] In the cyclic voltammogram of complex **6**, a reversible reduction wave can be seen at −1.49 V. This, after comparison with the cyclic voltammogram of **7**, can be attributed to reduction of the Pt(bpy) moiety. This assignment is further supported by the results of the DFT calculations on complex **6**, which show that the LUMO is clearly located on the bipyridyl part of the molecule.

Transient Absorption Spectroscopy. a. Dynamics of Parent Compounds. Initial experiments characterized the transient absorption kinetics of the free ligand, **1a** (see Supporting Information, Figure S1) and the Pt(bpy)(bdt) chromophore, **7** (Figure S2). After excitation at 530 nm, the TA spectra of **1a** are characterized by a bleach of the ground-state absorption at ∼530 nm and an excited-state absorption (ESA) band at ∼340 nm. There is little spectral evolution, and each of these features decays away with the characteristic 3−4 ns excited-state lifetime of the isolated Bodipy $^1\pi\pi^*$ state. The Pt chromophore **7** was excited at 615 nm. Its TA spectra (Figure S2) are characterized by a broad ESA signal extending to the blue from 510 nm and a ground-state (GS) bleach from 510 to 580 nm that shifts to higher energy over the first 2 ps. An additional ESA signal is initially seen at wavelengths greater than 600 nm but then blue shifts to $\lambda > 580$ nm over the first 1 ps. After 2 ps, the spectra are completely static. Hence, we attribute these rapid spectral shifts in the Pt chromophore to ISC from the ^{1}MMLL′CT state to the ^{3}MMLL′CT state, occurring with a 1 ± 0.7 ps time constant.

b. Dynamics of Dyad 3. Figure 4 shows the femtosecond transient absorption spectra for the Pt(**1a**)(bdt), dyad **3**. In contrast to the spectra of its parent compounds, the free ligand **1a** and the Pt(bpy)(bdt) chromophore **7**, the spectra of dyad **3** evolve dramatically over the first 50 ps. When the dyad is excited at 530 nm (Figure 4a), the spectra show an initial bleach of the Bodipy absorption band at probe wavelengths around 530 nm, as well as a negative signal at ∼600 nm attributable to Bodipy stimulated emission (SE). Over the first 2 ps, a dramatic decrease in the 530 nm bleach signal is observed, which is

(37) Ziessel, R.; Allen, B. D.; Rewinska, D. B.; Harriman, A. *Chem.—Eur. J.* **2009**, *15*, 7382–7393.
(38) Burghart, A.; Kim, H. J.; Welch, M. B.; Thoresen, L. H.; Reibenspies, J.; Burgess, K.; Bergstrom, F.; Johansson, L. B. A. *J. Org. Chem.* **1999**, *64*, 7813–7819.
(39) Mitsopoulou, C. A.; Dagas, C. E.; Makedonas, C. *J. Inorg. Biochem.* **2008**, *102*, 77–86.

Table 4. Results of Least-Squares Fit of Transient Absorption Kinetics[a]

compd	pump (nm)	probe (nm)	a_0 (ΔOD)	τ_0 (ps)	a_1 (ΔOD)	τ_1 (ps)	a_2 (ΔOD)	τ_2 (ps)	a_{step}
3	530	355	0.0105	0.28 ± 0.04	0.0044	12 ± 1			0.0005
		425	0.0026	0.7 ± 0.3	0.0041	10 ± 2			0.0082
		500	−0.0093	0.6 ± 0.1	0.0116	8.4 ± 0.8			−0.0128
		533	−0.0438	0.3 ± 0.2	0.0113	8 ± 1			−0.0383
		600	−0.0107	0.32 ± 0.04	−0.0053	6.6 ± 0.5			0.0021
	615	380	0.0257	0.30 ± 0.04	0.0049	9.0 ± 1			0.0082
		420	0.0208	0.28 ± 0.03	−0.0127	1.8 ± 0.2	−0.0137	18 ± 1	0.0392
		500	0.0365	0.92 ± 0.04	0.0817	7.96 ± 0.08			−0.0886
		600	−0.0224	0.6 ± 0.1	−0.0105	11.6 ± 0.6			0.0134
6	530	425	0.0056	0.6 ± 0.1					0.0069
		489	−0.0073	1.6 ± 0.3	0.0106	187 ± 47			−0.0133
		525	0.048	0.77 ± 0.06	−0.016	16 ± 7	0.034	142 ± 36	0.037
		600	−0.0032	0.5 ± 0.1	−0.0047	51 ± 8			0.0036
	600	380	0.0167	0.28 ± 0.02	0.0041	33 ± 4	0.0051	202 ± 30	0.0011
		440	0.0122	0.28 ± 0.03	−0.0109	141 ± 13			0.0170
		489	0.0461	160 ± 5					−0.0475
		535	0.0037	2.0 ± 0.4	0.0267	119 ± 6			−0.0132
		645	−0.0132	0.31 ± 0.02	−0.0056	134 ± 16			0.0136

[a] Parameters are determined by least-squares fitting of the convolution of the Gaussian instrument response with the sum of exponentials, presented here as $I(t > 0) = a_0\, e^{(-t)/(\tau_0)} + a_1\, e^{(-t)/(\tau_1)} + a_2\, e^{(-t)/(\tau_2)} + a_{step}$.

accompanied by a loss of ESA signal at ∼350 nm and decreasing signal at 600 nm. Between 2 and 10 ps, the bleach plateaus before increasing in magnitude again until 20−30 ps. The terminal spectrum is obtained by 30 ps and is characterized by a sharp ESA band at 425 nm and the GS bleach at ∼530 nm. The kinetic fits (Table 4) indicate that the rapid initial dynamics occur with a 0.28−0.30 ps time constant, as determined by the loss of Bodipy GS bleach and SE and the ESA band at 360 nm. The subsequent rebleaching of the Bodipy ground-state band, decrease in signal at 600 nm, and growth of the band at 425 nm all occur with a 6−8 ps time constants. We can assign the 425 nm absorption band to the Bodipy $^3\pi\pi^*$ state, based on previous microsecond transient absorption experiments performed separately by Rachford and Harriman.[40,41] The observation of this feature in the terminal transient absorption spectra of each species herein indicates that the Bodipy $^3\pi\pi^*$ state is the final electronic state accessed by the system on the picosecond time scale.

When excited at 615 nm, compound **3** (Figure 4b) exhibits dynamics similar to the ∼10 ps decay observed when pumped at 530 nm. The initial spectrum is very similar to that of model compound **7**: a broad ESA signal from 340 to 500 nm and a broad negative GS bleach around 600 nm. On the ∼10 ps time scale, the Bodipy ground-state absorption band is bleached, the ESA at 340 nm disappears, and the characteristic Bodipy $^3\pi\pi^*$ 425 nm absorption band is formed. This spectrum then remains constant for time delays up to 1.5 ns. As shown in Table 4, the initial dynamics at 380, 425, and 600 nm occur with time constants from 0.3 to 0.9 ps, consistent with a rapid ISC process from the photoexcited ^{1}MMLL′CT state to the ^{3}MMLL′CT state. The subsequent bleach of the Bodipy ground-state absorption band and the growth of the signal at 425 nm is dominated by a 8−18 ps time constant, though at 425 nm, ∼30% of the signal shows up more rapidly, with a 1.8 ps time constant.

c. Dynamics of Dyad 6. Figure 5 shows the evolving spectra of dyad **6** when excited at 530 or 600 nm. The evolution of the spectra very closely matches that observed for dyad **3** (Figure 4) but occurs on a different time scale. When the dyad is excited at 530 nm (Figure 5a), the initially strong bleach of the Bodipy absorption band recovers with a 0.8 ps time constant before subsequently "re-bleaching" with a 140 ps time constant. On the longer time scale, a new absorption band is formed between 400 and 450 nm, which closely resembles the Bodipy $^3\pi\pi^*$ 425 nm band observed for **3**. (The weaker signals at 360, 425, and 600 nm evolve with a broad range of time constants from 50 to 700 ps, the range of which we attribute to significant errors associated with fitting such weak signals.) When dyad **6** is excited at 600 nm (Figure 5b), the instantaneous bleach of the 530 nm absorption band is avoided, and the spectra up to 20 ps are characterized by a broad, featureless absorption band from

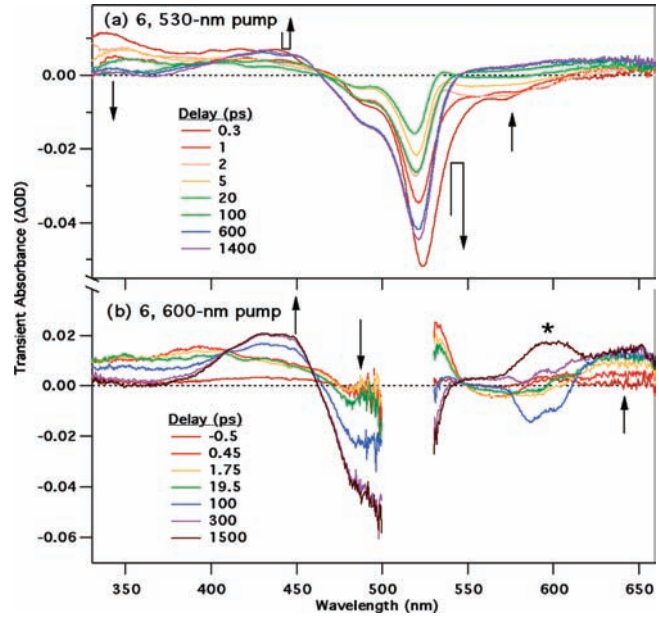

Figure 5. Femtosecond transient absorption spectra of **6**, following 530 (a) or 600 nm (b) excitation. In (b), the high OD of the sample at ∼515 nm prevented the observation of the spectra between 500 and 530 nm. The asterisk indicates a region of the spectrum where sporadic pump scattering contaminated the spectra.

(40) Rachford, A. A.; Ziessel, R.; Bura, T.; Retailleau, P.; Castellano, F. N. *Inorg. Chem.* **2010**, *49*, 3730–3736.
(41) Harriman, A.; Rostron, J. P.; Cesario, M. l.; Ulrich, G.; Ziessel, R. *J. Phys. Chem. A* **2006**, *110*, 7994–8002.

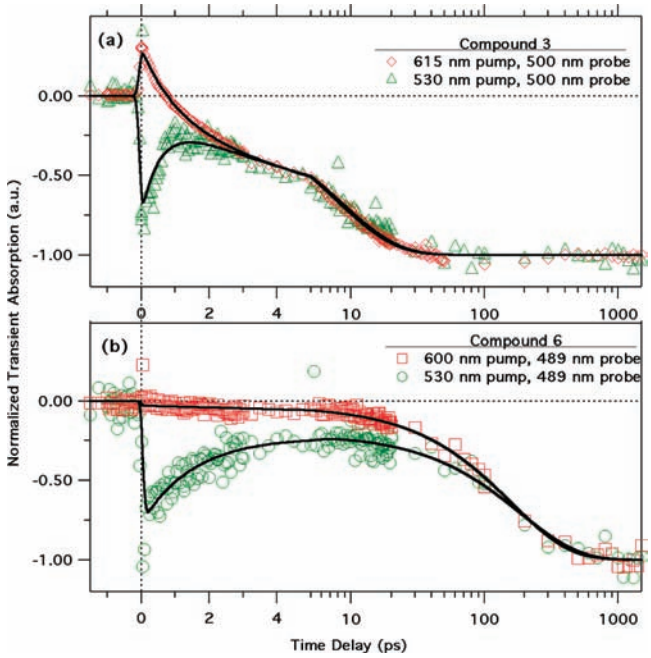

Figure 6. Kinetics of **3** (a) and **6** (b) at probe wavelengths of 500 and 489 nm, following excitation at 530 (green symbols) or 600 or 615 nm (red symbols). The kinetics at these probe wavelengths are indicative of the bleach of the Bodipy $\pi\pi^*$ absorption band. Lines are the kinetic fits as described in Table 4. Note that the time axis is linear to 5 ps and logarithmic from 5 to 1500 ps. The intensities have been normalized to have equivalent bleach at long times.

340 to 475 nm and around 650 nm. Subsequently, the broad ESA band is replaced by the sharp $^3\pi\pi^*$ feature from 400 to 450 nm and the Bodipy GS bleach at 500 nm, which grow in with 140−160 ps time constants.

Figure 6 compares the kinetics of the Bodipy bleach signal when **3** and **6** are excited at 530 and 600/615 nm. When **3** is excited at 615 nm (Figure 6a, red), the GS bleach of the Bodipy chromophore grows in exponentially with an 8 ps time constant. When **3** is excited at 530 nm (Figure 6a, green), the Bodipy GS bleach appears instantaneously at $\Delta t = 0$, recovers with a 0.28 ps time constant, and then subsequently "re-bleaches" with an 8.2 ps time constant. When dyad **6** is excited by the 530 nm pump (Figure 6b, green), the Bodipy GS bleach appears instantaneously and then recovers with a 1.6 ps time constant before finally "re-bleaching" in 187 ps. When dyad **6** is excited at 600 nm (Figure 6b, red), the instantaneous bleach at 530 nm is not present, but the longer time scale bleach still occurs, now with a 160 ps time constant.

d. Dynamics in Dyad 4. In **4**, Bodipy-Pt(**1a**)(mnt), the mnt ligand shifts the MMLL′CT absorption band to higher energy, so that it lies almost directly under the Bodipy $\pi\pi^*$ absorption band. Hence, 530 nm excitation should primarily excite the Bodipy $^1\pi\pi^*$ state, but some direct excitation of the Pt chromophore via the underlying ^{1}MMLL′CT absorption may occur. However, the TA kinetics are all consistent with excitation only to the Bodipy $\pi\pi^*$ state (see Supporting Information, Figure S3). In the spectra 0.5 ps after excitation, a strong bleach of the Bodipy $\pi\pi^*$ absorption band at 530 nm is present, along with a negative SE band from 570 to 620 nm and a broad ESA band from <340 to 460 nm. Over the course of the first 1.5 ps, a rapid loss of the bleach and SE signals occurs, with 0.5 and 1.9 ps time constants (Figure S3, inset). At 2 ps, the bleach magnitude begins to increase and a sharp ESA peak at 425 nm appears with 5 and 4 ps time constants, respectively, after which the spectrum is constant on the nanosecond time scale.

e. Dynamics in Dyad 2. For the Pt(**1a**)Cl_2 complex **2**, the charge-transfer state occurs at high enough energy so that it is not directly excited by the 530 nm pump pulse. Instead, as shown in Figure S4 (Supporting Information), 530 nm excitation directly excites the Bodipy $^1\pi\pi^*$ state, apparent in the instantaneous appearance of the 530 nm GS bleach, the 570−620 nm SE band, and the broad ESA from <330 to 460 nm. Over the first 5 ps, the bleach and SE signals are significantly attenuated, with 4.5 ps time constants, and the SE band red shifts to a distinct feature at 610 nm. After this initial reorganization, the SE band disappears with a 680 ps time constant, and the sharp ESA at 425 nm appears with a 290 ps time constant, as measured by the loss of absorption signal at 445 nm.

DFT Calculations. The frontier orbital diagrams were generated for the model complexes **1a′**, **2′**, **3′**, **4′**, and **7′** from the optimized geometries. **1a′**−**7′** are equivalent to **1a**−**7**, except that all of the peripheral alkyl groups have been treated as methyls. Time-dependent DFT calculations were performed to determine the transitions involved in the lowest energy states. The parameters for the optimized geometries and full list of excited states are included in the Supporting Information. The long-range-corrected B3LYP level of theory was used to eliminate the physically unrealistic low energy charge transfer states. Both singlets and triplets were calculated, and the lowest energy and highest oscillator strength vertical transitions are summarized in Table 5 and Figure 7. States with no oscillator strength and unclear assignments are not included in the analysis, for instance S_3, S_4, and S_5 in **2′**, since there is no evidence for these additional states in the experimental data.

The ligand **1a′** possesses a HOMO that is of Bodipy π character and a LUMO that is a Bodipy-based π^* orbital. The TD-DFT calculation shows a lowest energy singlet transition of HOMO→LUMO character with a high oscillator strength of 0.55 and energy of 2.89 eV. This Bodipy-based $\pi\pi^*$ transition appears in the Pt complexes as well, although not as the lowest energy singlet excited state.

The model Pt complex with no Bodipy, **7′**, shows frontier orbitals where the HOMO and HOMO-1 are of mixed Pt and dithiolate character, whereas the lowest unoccupied orbitals are of bpy π^* character (see Supporting Information). The lowest triplet and singlet transitions in **7′** are therefore charge transfers from the HOMO to the LUMO frontier orbitals, which have previously been assigned as MMLL′CTs. The lowest singlet state has a calculated energy of 2.14 eV and an oscillator strength of 0.14. This type of MMLL′CT transition also appears in complexes **3′** and **6′**.

As shown in Figures 8 and 9, for dyad complexes **3′** and **6′**, in which the Bodipy is connected to the either the diimine or the dithiolate, the frontier orbitals consist of both mixed Pt−dithiolate orbitals similar to those calculated for complex **7′** and Bodipy π and π^* orbitals seen in ligand **1a′**. In complex **3′** the LUMO lies on the Bodipy unit. The lowest triplet transition is primarily HOMO-2 to LUMO, corresponding to a Bodipy $^3\pi\pi^*$ excited state at 1.12 eV. Additional geometry optimization of the lowest triplet state shows that there are minimal geometrical changes between the ground-state and $^3\pi\pi^*$ structures and confirms that this state remains the lowest energy triplet state, even away from the vertical transition geometry. The lowest energy singlet transition (2.17 eV) is HOMO to LUMO+1, which possesses mixed Pt−dithiolate and bpy π^*

Table 5. TD-DFT Calculated Energies, Oscillator Strengths, and Percent Contributions from Dominant One-Electron Excitations for the Most Relevant Excited Electronic States

compd	state	*E* (eV) calcd	obsvd[a]	calc'd *f*	transition	assignment
1a′	T_1	1.20		0	98% HOMO→LUMO	Bodipy $^3\pi\pi^*$
	S_1	2.89	2.34	0.55	100% HOMO→LUMO	Bodipy $^1\pi\pi^*$
2′	T_1	1.13		0	98% HOMO→LUMO	Bodipy $^3\pi\pi^*$
	T_2	2.65		0	63% (HOMO-1)→(LUMO+1)	$PtCl_2$→bpy ^{3}MLCT
	S_1	2.85	2.31	0.54	100% HOMO→LUMO	Bodipy $^1\pi\pi^*$
	S_6	3.37	∼3.15	0.11	95% (HOMO-2)→(LUMO+1)	$PtCl_2$→bpy ^{1}MLCT
3′	T_1	1.12		0	88% (HOMO-2)→LUMO	Bodipy $^3\pi\pi^*$
	T_2	1.78		0	96% HOMO→(LUMO+1)	Pt(bdt)→bpy ^{3}MMLL′CT
	S_1	2.17	2.08	0.17	100% HOMO→(LUMO+1)	Pt(bdt)→bpy ^{1}MMLL′CT
	S_4	2.90	2.31	0.54	84% (HOMO-2)→LUMO	Bodipy $^1\pi\pi^*$
4′	T_1	1.11		0	98%(HOMO-1)→(LUMO+1)	Bodipy $^3\pi\pi^*$
	T_2	2.04		0	94% HOMO→LUMO	Pt(mnt)→bpy ^{3}MMLL′CT
	S_1	2.39		0.15	100% HOMO→LUMO	Pt(mnt)→bpy ^{1}MMLL′CT
	S_3	2.85	2.30	0.54	100%(HOMO-1)→(LUMO+1)	Bodipy $^1\pi\pi^*$
6′	T_1	1.25		0	77% HOMO→(LUMO+1)	Bodipy $^3\pi\pi^*$
	T_2	1.95		0	80% (HOMO-1)→LUMO	Pt(bdt)→bpy ^{3}MMLL′CT
	S_1	2.33	2.18	0.17	83% (HOMO-1)→LUMO	Pt(bdt)→bpy ^{1}MMLL′CT
	S_4	2.95	2.37	0.45	71% HOMO→(LUMO+1)	Bodipy $^1\pi\pi^*$
7′	T_1	1.75		0	94% HOMO→LUMO	Pt(bdt)→bpy ^{3}MMLL′CT
	S_1	2.15	2.21	0.14	100% HOMO→LUMO	Pt(bdt)→bpy ^{1}MMLL′CT

[a] Observed vertical excitation energies are calculated from the absorption maxima in Table 2.

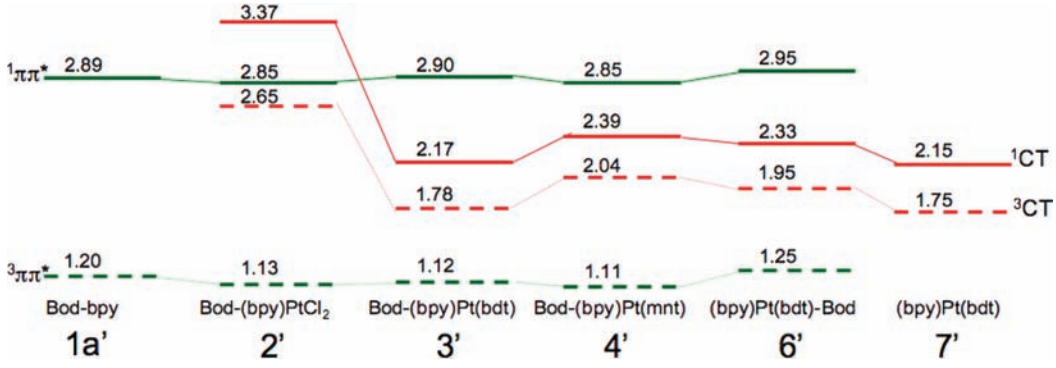

Figure 7. Energy level diagrams for compounds **1a′**−**4′**, **6′**, and **7′**, with the energy levels determined by TD-DFT calculations. Solid lines refer to singlet states and dotted lines to triplet states. Green lines refer to the Bodipy $\pi\pi^*$ states, and red lines refer to the charge transfer (CT) states of the $PtCl_2$, complex **2′**, or the MMLL′CT states of the Pt−dithiolate complexes **3′**, **4′**, **6′**, and **7′**.

character, respectively. Thus, the lowest energy transition in **3′** is MMLL′CT-based, which correlates well to the lowest singlet state found in complex **7′** that has an energy of 2.15 eV. The Bodipy-based $^1\pi\pi^*$ transition is a higher energy singlet state with a high oscillator strength and an energy of 2.90 eV, which is very close to the first singlet transition of ligand **1a′** (2.89 eV). The lowest lying triplet-state transition of **3′** is Bodipy-based $^3\pi\pi^*$. This supports the TA observation of the Bodipy-based triplet becoming populated after excitation of the low-lying MMLL′CT transition since the $^3\pi\pi^*$ is lower in energy.

When the Bodipy moiety is connected to the dithiolate in complex **6′,** the HOMO and HOMO-1 levels are only separated by ∼0.09 eV and are of Bodipy and Pt-bdt character, respectively (see Figure 9). The LUMO of **6′** is bpy-centered, and the much higher LUMO+1 is of Bodipy π^* character. The lowest lying triplet transition is 77% HOMO to LUMO+1, or Bodipy $^3\pi\pi^*$. The second triplet state is primarily ^{3}MMLL′CT in character, from the Pt(bdt) HOMO-1 to the bpy π^* LUMO, as is the lowest lying singlet excited state at 2.33 eV with an oscillator strength of 0.17. This is 0.18 eV higher in energy than the ^{1}MMLL′CT state of the model compound **7′**. Interestingly, each of these MMLL′CT states contains significant contributions (15−17%) from a Bodipy-to-bpy charge-transfer, HOMO→LUMO excitation. The Bodipy $^1\pi\pi^*$ state is at 2.95 eV with an oscillator strength of 0.45, consistent with the energy calculated for ligand **1a′** and complex **3′**.

When the benzenedithiolate ligand (bdt^{2-}) is changed to a maleonitriledithiolate ligand (mnt^{2-}), as in **4′**, the absorption spectrum indicates that the ^{1}MMLL′CT is shifted to a higher energy by the absence of a low-energy shoulder (Figure 4). The calculation on complex **4′** supports this observation, as the lowest energy singlet transition lies 0.22 eV higher in energy than the equivalent transition calculated for complex **3′**. However, TD-DFT calculations show the ^{1}MMLL′CT of **4′** to be only 0.06 eV above that of **6′**, which contrasts with the experimental UV−vis spectrum that exhibits a distinct low-energy shoulder in **6′** and none in **4′**. Instead, the lack of an observable shoulder in **4′** is due to the simultaneous lowering

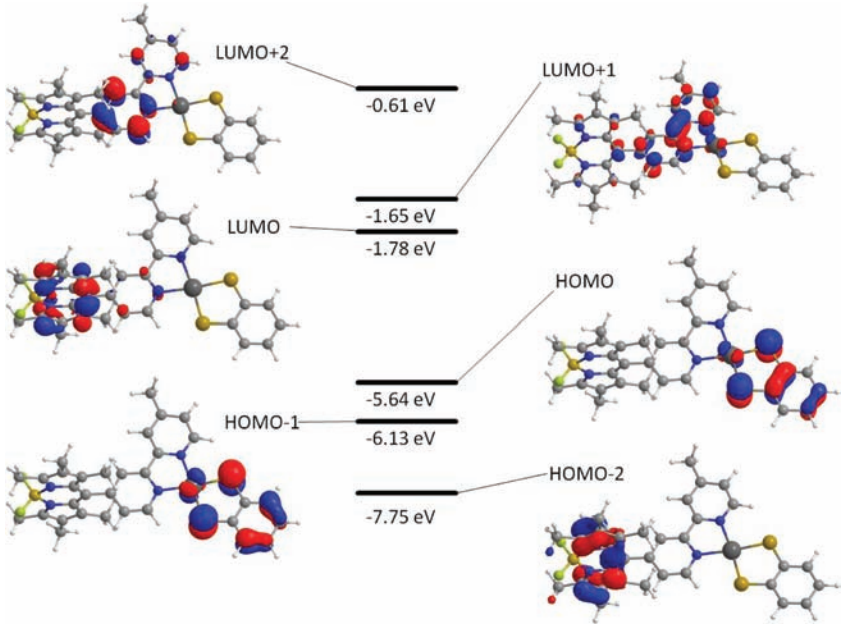

Figure 8. Molecular orbital diagrams and energies for the frontier orbitals of the Pt(**1a**)(bdt) dyad **3′**.

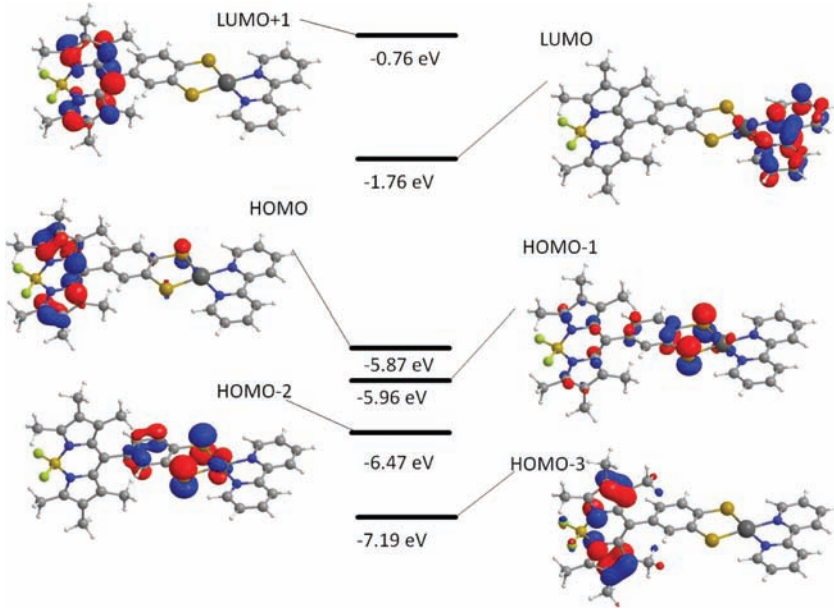

Figure 9. Molecular orbital diagrams and energies for the frontier orbitals of the (bpy)Pt(bdt)−Bodipy dyad **6′**.

of the Bodipy $^1\pi\pi^*$ state and the raising of the ^{1}MMLL′CT state, reducing the computed energy gap between them to just 0.46. In **3′** and **6′**, this energy gap is significantly larger, at 0.73 and 0.62 eV, respectively.

In the calculation for complex **2′**, the presence of two chloride ligands on Pt instead of a dithiolate ligand lowers the energy of the Pt-based orbitals, resulting in a Bodipy-based HOMO. The LUMO and LUMO+1 of **2′** are very close in energy ($\Delta E \approx 0.04$ eV) and are of Bodipy π^* and bpy π^* character, respectively. The TD-DFT calculations indicate that the lowest energy singlet transition is of Bodipy $\pi\pi^*$ character at 2.85 eV, which is slightly red-shifted compared to the equivalent transition of ligand **1a′** (2.89 eV). The MLCT Pt-to-bpy transition in **2′** has a calculated energy of 3.37 eV and an oscillator strength of 0.1. This is much higher in energy than the MMLL′CT transitions for the Pt−dithiolate complexes.

Discussion

The photophysics of **3** and **6**, containing a Bodipy chromophore covalently linked to either the bipyridyl ligand (**3**) or benzenedithiolate ligand (**6**) of the Pt(bpy)(bdt) chromophore, can be understood using the energy level diagram shown in Figure 10. In each case, absorption of 530 nm light excites the system to the $^1\pi\pi^*$ state localized on the Bodipy chromophore. In the case of the bare Bodipy-bpy chromophore **1a**, the molecule stays in the $\pi\pi^*$ state for several nanoseconds, decaying via radiative and nonradiative decay to the ground state with negligible ISC to the $^3\pi\pi^*$ state. However, in the presence of the Pt(bpy)(dithiolate) chromophore, the $^1\pi\pi^*$ state

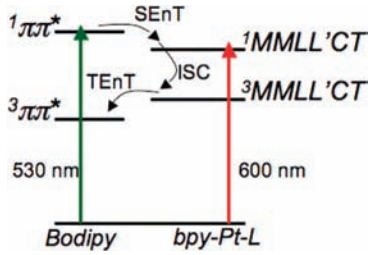

Figure 10. Energy level diagram relevant to the photochemistry of **3** and **6**.

depopulates rapidly, in 0.6 ps for **3** and 1.6 ps in **6**, as evidenced by the rapid recovery of the Bodipy TA bleach at 525−530 nm and the quenching of Bodipy fluorescence in the dyads. We interpret the fast TA decay as evidence of population of the ^{1}MMLL′CT state of the Pt chromophore via singlet energy transfer (SEnT, Figure 10). One could describe this process as intramolecular "internal conversion" as well, but given the lack of coupling between the various electronic states, as seen in the UV−vis spectrum of Figure 4, we think that this process is better described as "energy transfer" between two isolated chromophores.

As shown in Figure 6, after the initial SEnT process, the kinetics of **3** and **6** behave the same whether the dyad is excited at 530 or 600/615 nm. This is evidence that the state populated after excitation at 530 nm and subsequent rapid SEnT is the same as that which is directly populated by optical excitation at 600/615 nm, namely the ^{1}MMLL′CT state. After the ^{1}MMLL′CT state is populated, it undergoes rapid ISC as a result of the large spin−orbit coupling associated with the Pt(II) ion. TA spectra of **7** indicate that this rapid ISC occurs in <1 ps and produces only subtle changes in the spectrum (Supporting Information, Figure S2). In **3**, the weak TA signatures of the ^{1}MMLL′CT and ^{3}MMLL′CT states (Figure S2) and the rapid spectral evolution of the system make positive identification of this state difficult. However, the spectrum of **6** at $\Delta t = 20$ ps (Figure 5) matches that of the directly photoexcited Pt(bpy)(bdt) compound **7** at $\Delta t > 5$ ps, supporting our assignment of the initial relaxation as $^1\pi\pi^*$ to ^{1}MMLL′CT SEnT, followed by ISC to the ^{3}MMLL′CT state.

After relaxation to the ^{3}MMLL′CT state, dramatic spectral changes occur in both the spectra of **3** and **6**, namely the rebleaching of the Bodipy ground-state absorption band and the formation of the distinctive ESA peak at 425 nm in **3** and 440 nm in **6**. The 425 nm absorption band has been definitively assigned to the $^3\pi\pi^*$ state on Bodipy[41] and is naturally accompanied by a bleaching of the Bodipy ground-state absorption band. Hence the final process observed on this time scale is the triplet energy transfer (TEnT) from the ^{3}MMLL′CT to the $^3\pi\pi^*$ state, which occurs in 8 ps in **3** and 160 ps in **6**.

In **4**, with maleonitriledithiolate (mnt) in place of the benzenedithiolate (bdt) ligand of dyad **3**, the energy of the ^{1}MMLL′CT state increases to near degeneracy with the Bodipy $^1\pi\pi^*$ state. This raises the possibility that the initial SEnT process might be endothermic and therefore greatly reduced or eliminated. However, the TA spectra in Figure S3 (see Supporting Information) show that **4** follows essentially the same relaxation pathway as **3**. Initial excitation places the system in the $^1\pi\pi^*$ state, which decays in ∼0.5 ps, presumably populating the ^{1}MMLL′CT by SEnT. The Bodipy GS bleach reappears with a ∼5 ps time constant after the initial loss of intensity and is accompanied by growth of the distinctive $^3\pi\pi^*$ absorption at 425 nm. Given the radiative rate of **1a** ($k_{rad} = 0.14$ ns^{-1}), the 0.5 ps fluorescence lifetime of **4** indicates a fluorescence quantum yield of only 7×10^{-5}. However, a small but significant ($\Phi = 0.004$) fluorescence at 594 nm is observed. This may be due to a small portion of thermal structural configuration fluctuations that prevent rapid SEnT and thereby facilitate radiative decay, or it may be due to a small amount of contaminant.

In **2**, the presence of two chloride ligands instead of the benzenedithiolate of **3** moves the CT-to-diimine transition to the near-UV region of the spectrum. Hence, the SEnT process shown in Figure 10 is no longer possible since the CT states are too high. Instead, rapid reorganization in the $^1\pi\pi^*$ state for **2** is seen that red-shifts the SE band to ∼600 nm and decreases the magnitude of the negative transient absorption signal around 530−600 nm with a ∼4 ps time constant (see Supporting Information, Figure S4). On a longer time scale, the SE band at 600 nm decays and the 420 nm ESA of the $^3\pi\pi^*$ state appears, with time constants from 290 to 680 ps. Hence, in **2**, ISC directly from $^1\pi\pi^*$ to $^3\pi\pi^*$ is facilitated by the presence of the Pt(II) atom, but without direct population of the Pt ion-containing CT states. In particular, the lack of loss and subsequent recovery of the Bodipy GS bleach indicates that the excitation remains localized on the Bodipy moiety throughout the relaxation process. The 290−680 ps lifetime of the $^1\pi\pi^*$ state, as determined by the TA absorption, is sufficient to allow the rather large fluorescence quantum yield (0.33) observed in the steady-state experiments (Table 2).

Mechanism of Energy Transfer in 3 and 6. The rapidity of the singlet and triplet energy-transfer steps in **3**, **4**, and **6** is quite striking. Dyad complexes **3** and **6** offer insights into the mechanism of SEnT and TEnT because they incorporate exactly the same chromophores and differ only in their structural orientation. Both dyads **3** and **4** (with the Bodipy on the diimine) undergo energy transfer signficantly more quickly than **6** (with the Bodipy on the dithiolate). The strong overlap between the Bodipy fluorescence and the MMLL′CT absorption bands indicates a propensity for Förster-type fluorescence resonance energy transfer (FRET).[42] We can calculate a predicted FRET rate, k_{FRET}, using

$$k_{FRET} = \frac{1}{\tau_D}\left(\frac{R_0}{r_{DA}}\right)^6 \quad (1)$$

in which τ_D is the fluorescence lifetime of the donor, r_{DA} is the donor−acceptor distance, and R_0 is the Förster distance that is a measure of the coupling between the donor and acceptor transition dipoles. The Förster distance is calculated using

$$R_0^6 = \Phi_D \kappa^2 J(\lambda) \quad (2)$$

Here, Φ_D is the donor fluorescence quantum yield in the absence of the acceptor, κ^2 is related to the relative orientation of the donor and acceptor transition dipoles, and $J(\lambda)$ is the spectral overlap integral between the emission spectrum of the donor and the absorption spectrum of the acceptor. Quantitatively, the spectral overlap between the emission of **1a** and the absorption of **7** predicts a Förster distance, R_0, of 41.6 Å if the chromophores are assumed to have a dynamically averaged orienta-

(42) Lakowicz, J. R. *Principles of Fluorescence Spectroscopy*, 2nd ed.; Kluwer/Plenum: New York, 1999.

tion ($\kappa^2 = 2/3$).[42,43] Taking the donor−acceptor distance as the distance between the B and Pt atoms, **3** has an $r_{DA} = 9.35$ Å and therefore a predicted FRET time constant of 0.4 ps (using $\tau_{fl,D} = 3$ ns from transient absorption). Likewise, **6** has an $r_{DA} = 9.94$ Å and a predicted FRET time constant of 0.6 ps. The experimentally observed $^1\pi\pi^*$ lifetimes are 0.6 and 1.6 ps for **3** and **6**, respectively, when excited at 530 nm and probed on the blue side of the GS bleach (500 or 489 nm), which agree quite well in trend and overall magnitude with the computed FRET time constants. However, we cannot attribute the increase in $^1\pi\pi^*$ lifetime in **6** to simply an increase in the donor−acceptor distance because of several issues with this mechanism. First, a dipole−dipole approximation for the coupled transition dipoles is not appropriate for two chromophores in such close proximity. Instead, a transition density coupling would be more accurate and would likely produce a significantly longer lifetime.[44] Second, the two chromophores in the dyads are far from orientationally averaged, since there is significant steric hindrance about the C−C bond connecting them. In the DFT structures, the Bodipy $S_0 \rightarrow {}^1\pi\pi^*$ transition dipole is nearly perpendicular to $\vec{r}_{DA}$, and the transition dipole to the ^{1}MMLL′CT state is tilted by 20−30° relative to $\vec{r}_{DA}$. Because of this, the orientational factor, κ^2, is only 4×10^{-4} in **3** and 5×10^{-8} in **6**; in other words, the orientation of the two transition dipoles prevents effective coupling between them. This increases the predicted time constant for energy transfer to 710 ps in **3** and 7.8 μs in **6**, though structural fluctuations will increase the coupling and reduce the time constants somewhat. This analysis suggests that, when the details of the FRET mechanism are inspected, it cannot account for the extremely rapid rate of energy transfer observed in **3** and **6**. Instead, we think that relaxation from the $^1\pi\pi^*$ to ^{1}MMLL′CT state must occur via an electron exchange (Dexter) mechanism.[45,46]

After rapid ISC within the MMLL′CT manifold, we see that the TEnT back to the Bodipy $^3\pi\pi^*$ state also proceeds extraordinarily quickly, occurring with an 8.2 ps time constant in **3** and a 160 ps time constant in **6**. In this case, the negligible transition dipoles for the S_0 to triplet-state transitions mean that FRET is not possible; TEnT must necessarily proceed via an electron exchange mechanism.[47] However, unlike typical photochemical excited state species in which the electron and hole are tightly bound in overlapping regions of space, the presence of the MLCT states here dictates that we consider the separate dynamics of the electron and hole. For instance, in the initial relaxation from the $^1\pi\pi^*$ state to the ^{1}MMLL′CT state in **3**, the excited electron need only move from the Bodipy π^* orbital to the bpy π^* orbital, but the hole needs to migrate from the Bodipy π orbital all the way to the PtS_2 metal−ligand orbital. For the same relaxation in **6**, the hole has a short migration from the Bodipy π to the PtS_2 metal−ligand bond, but the excited electron needs to move from the Bodipy π^* orbital to the distant bpy π^*. Because of this, it is important to consider these as potentially separate electron transfer (eT) processes that may occur in either a sequential or concerted manner.[46] To examine this, we have calculated the energies of the corresponding eT intermediates using Weller's dielectric continuum method, including the corresponding redox potentials of **3** and **6**.[48,49] As shown in Table 3, in **3** (**6**), the PtS_2 moiety is oxidized at +0.61 V (0.55 V), Bodipy is oxidized at +1.09 V (+0.95 V), and bpy is reduced at −1.08 V (−1.49 V). For each species, we consider the reduction potential of Bodipy to be −1.30 V, as measured for **1a** and in agreement with previous measurements.[50] The eT distances were calculated from the DFT structures of **3** and **6**. The center of the Bodipy π and π^* orbitals was taken as between the two nitrogens of Bodipy; the center of the bpy π^* orbital was taken as being between the central carbons linking the pyridyls; the center of the PtS_2 metal−ligand orbital was taken as between the two sulfurs. Defined in this manner, the Bodipy−bpy distance is 8.19 Å (11.87 Å) in **3** (**6**), and the Bodipy−PtS_2 distance is 9.84 Å (7.71 Å). On average, these values agree with the previous calculated $\pi\pi^*$ to MMLL′CT distances of 9.35 Å for **3** and 9.94 Å for **6**. When combined with redox potentials, these values can be used to estimate the energy of a charge-separated species in a dielectric continuum.

However, in addition to having slightly different effective electron exchange distances, there is a qualitative difference in the electronic coupling occurring in **3** and **6**. In Figure 8, we see that for **3** the close proximity of the bpy and Bodipy moieties produces electronic orbitals in which the primarily bpy π^* LUMO+1 orbital has significant orbital amplitude on the Bodipy. Likewise, the Bodipy π^* LUMO orbital has some density on the carbons of the bpy. Because of this, we can expect strong coupling that will enhance the rate at which the electron can move between these orbitals. In contrast, the hole must move between the HOMO (PtS_2 ML) and HOMO-2 (Bodipy π), which are spatially isolated from each other and will therefore have a small electron exchange integral and decreased rate of eT. The opposite is true for **6** (see Figure 9), in which the proximity of the Bodipy and Pt(bdt) moieties produces significant overlap between the primarily PtS_2 ML HOMO-1 orbital and the Bodipy π HOMO. However, the bpy π^* LUMO of **6** is completely spatially isolated from the Bodipy π^* LUMO+1 orbital. Hence, in **6** we expect there to be enhanced hole transfer rates between Bodipy and PtS_2 relative to the eT rates between Bodipy and bpy. This has important implications for the mechanism of SEnT and TEnT in these systems, because it implies that the Dexter-type electron exchange should not proceed in a concerted manner, in which the electron and hole move simultaneously. Instead, for Dexter-type EnT, these dyads should proceed via a charge-separated (CS) intermediate, in which the faster charge carrier (e^- in **3** and h^+ in **6**) jumps to its destination and is followed by a lagging slow charge carrier (h^+ in **3** and e^- in **6**). Even though the CS intermediate is only fleetingly populated, and hence not detected in our data, we postulate that its energy critically determines the overall EnT rate.

Figure 11 shows the calculated energies of the CS intermediates that may occur during SEnT and TEnT along with the experimentally determined energies of the $\pi\pi^*$ and MMLL′CT states. In the SEnT of **3**, the enhanced rate of electron transfer relative to hole transfer will increase the likelihood of the pathway that proceeds through the Bodipy$^{(+)}$−bpy$^{(-)}$−PtS_2 intermediate, which is also the CS species closest in energy to the $^1\pi\pi^*$ and ^{1}MMLL′CT states. During the ^{3}MMLL′CT to $^3\pi\pi^*$ TEnT process, the rapid eT rate from the strong LUMO/LUMO+1 overlap will increase the likelihood of the pathway

(43) Förster, T. *Ann. Phys.* **1948**, *437*, 55–75.
(44) Czader, A.; Bittner, E. R. *J. Chem. Phys.* **2008**, *128*, 035101.
(45) Dexter, D. L. *J. Chem. Phys.* **1953**, *21*, 836–850.
(46) Turro, N. J. *Modern Molecular Photochemistry*; University Science Books: Sausalito, CA, 1991.
(47) Vura-Weis, J.; Abdelwahed, S. H.; Shukla, R.; Rathore, R.; Ratner, M. A.; Wasielewski, M. R. *Science* , *328*, 1547–1550.
(48) Greenfield, S. R.; Svec, W. A.; Gosztola, D.; Wasielewski, M. R. *J. Am. Chem. Soc.* **1996**, *118*, 6767–6777.
(49) Weller, A. *Z. Phys. Chem.−Wiesbaden* **1982**, *133*, 93–98.
(50) Galletta, M.; Puntoriero, F.; Campagna, S.; Chiorboli, C.; Quesada, M.; Goeb, S.; Ziessel, R. *J. Phys. Chem. A* **2006**, *110*, 4348–4358.

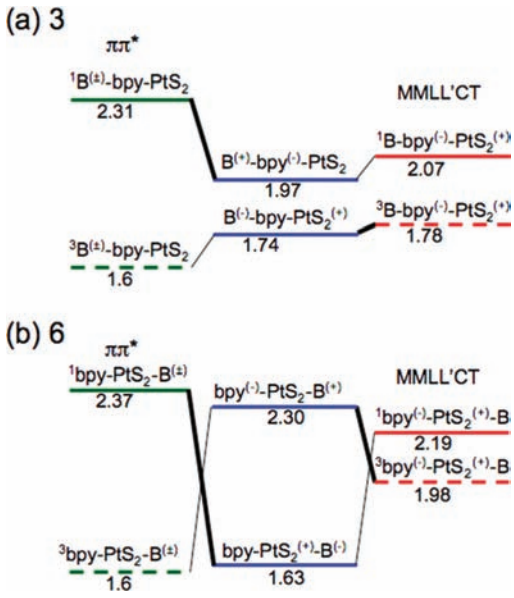

Figure 11. Experimental energies of the occupied states of (a) **3** and (b) **6** with the calculated energies of the potential charge-separated intermediate states (blue, other colors, and solid/dashed lines denote the same states as in Figure 7). Superscript (+) and (−) symbols indicate the presence of the hole and electron in each electronic configuration (B = Bodipy π or π^*, bpy = bipyridine π^*, PtS_2 = metal−ligand orbital of the dithiolate). Energies of each state are determined from absorption and emission wavelengths from this work and the Bodipy $^3\pi\pi^*$ emission from Galletta et al.[50] Energies of charge-separated intermediate states are calculated using Weller's dielectric continuum model.[49] The width of the diagonal lines connecting the states denotes the strength of the orbital overlap that couples them (see text). In **3**, the strong coupling and close energetic resonance of the electron exhange intermediates serve to enhance the energy-transfer rates relative to **6**.

through the Bodipy$^{(-)}$−bpy−$PtS_2^{(+)}$ intermediate, which again is the CS species that is closest in energy to the ^{3}MMLL′CT and $^3\pi\pi^*$ states. Hence in **3**, the energetics and electronic coupling work cooperatively to provide a fast and efficient pathway for electron exchange between the $\pi\pi^*$ and MMLL′CT states. In **6**, however, the energetically favorable intermediates are at odds with the strongly coupled intermediates. For the SEnT process in **6**, the strong coupling between the HOMO and HOMO-1 will enhance the probability of electron exchange utilizing the bpy−$PtS_2^{(+)}$−Bodipy$^{(-)}$ intermediate. However, this is the low-energy CS species with an energy that is far from resonance with the $^1\pi\pi^*$ and ^{1}MMLL′CT states. In the TEnT from ^{3}MMLL′CT to $^3\pi\pi^*$, the strong coupling for hole transfer will tend to favor the bpy$^{(-)}$−PtS_2−Bodipy$^{(+)}$ intermediate, which is a high-energy intermediate far from resonance with the initial and final triplet states. Hence, if EnT in **6** occurs by a superexchange mechanism, the system is forced to utilize either the poorly resonant intermediate with strong electronic coupling or the strongly resonant intermediate with weak electronic coupling. If the EnT processes occur via an incoherent eT hopping process, in which the CS species is actually populated, then energy conservation dictates that the system utilize an intermediate state in which poor electronic coupling will limit the EnT rate. In **3**, the cooperative effects of the resonance and strong coupling of the intermediate states accelerate the rate of energy transfer. But in **6** the resonant intermediate states lack strong coupling, which slows down the EnT process.

In previous work, similar Pt(diimine)(dithiolate) species have been used as dye sensitizers for solar hydrogen production and photovoltaics by incorporating a carboxylate linker between the bipyridine and TiO_2 particles.[51,52] Using this same motif, **6** can be incorporated into a dye-sensitized solar cell, in which case the greatly increased absorptivity of the Bodipy will improve the Pt-compound's visible-light harvesting abilities. Electron injection into TiO_2 would be expected to proceed from the Pt ^{1}MMLL′CT or ^{3}MMLL′CT states with near unity quantum yield because of the known subpicosecond injection times from similar MLCT sensitizers, and the relatively slow rate of the competing TEnT.[53,54] However, it is possible that even the low energy Bodipy $^3\pi\pi^*$ state could also support downhill electron injection, depending on its precise energy and the degree of proximity and coupling to the semiconductor.

Although the current dyads invoke a Dexter mechanism for EnT, the 41.6 Å Förster distance indicates that efficient Förster-type FRET may occur when the two chromophores are much farther apart than in the current scheme. This may provide a pathway for incorporating a variety of different light-harvesting dyes that are all tethered via relatively long covalent linkages to a single Pt(diiimine)(dithiolate). Such an array of light-harvesting dyes could be chosen to enhance spectral coverage of the solar spectrum, with energy absorbed in a variety of spectral regions all being funneled into the Pt chromophore that is bound to the surface of a TiO_2 particle in a photovoltaic or hydrogen producing solar cell.

Conclusions

Three new dyads, **3**, **4**, and **6**, combining Bodipy and Pt(diimine)(dithiolate) chromophores, have been prepared and characterized, and their photophysical and electrochemical properties have been investigated. Despite the strong luminescence of their constituent chromophores, **3** and **6** exhibit no emission, while **4** is very weakly emissive. Femtosecond transient absorption spectroscopy of the dyads and their model compounds, **1a**, **2**, **5**, and **7**, shows that initial excitation into the Bodipy-based $^1\pi\pi^*$ state is followed by rapid energy transfer to the ^{1}MMLL′CT excited states of the Pt(dithiolate) units, which, in turn, readily undergo intersystem crossing to the ^{3}MMLL′CT excited states due to the presence of the Pt(II) ion. These ^{3}MMLL′CT states, instead of undergoing radiative decay, engage in TEnT to the low-lying Bodipy $^3\pi\pi^*$ state. The increased rate of both singlet and triplet energy transfer in **3** relative to **6** is attributed to the improved resonance and electronic coupling of the charge-transfer intermediates in **3**. Gas-phase DFT and TD-DFT calculations of the studied compounds agree with the assignment of the transitions.

Sensitizing the charge-transfer state of the Pt(bpy)(bdt)-type chromophore as a method to increase light absorption for use in light-harvesting systems is an attractive proposition. However, from this work it is clear that many paths for electron transfer are present in these complicated systems that can result in unexpected routes for excited-state relaxation, resulting in loss of the desired properties of the exited CT state. We have shown that, through manipulation of the structural arrangement of the

(51) Zhang, J.; Du, P.; Schneider, J.; Jarosz, P.; Eisenberg, R. *J. Am. Chem. Soc.* **2007**, *129*, 7726–7727.
(52) Islam, A.; Sugihara, H.; Hara, K.; Singh, L. P.; Katoh, R.; Yanagida, M.; Takahashi, Y.; Murata, S.; Arakawa, H.; Fujihashi, G. *Inorg. Chem.* **2001**, *40*, 5371–5380.
(53) Kitamura, T.; Ikeda, M.; Shigaki, K.; Inoue, T.; Anderson, N. A.; Ai, X.; Lian, T.; Yanagida, S. *Chem. Mater.* **2004**, *16*, 1806–1812.
(54) Anderson, N. A.; Lian, T. *Annu. Rev. Phys. Chem.* **2005**, *56*, 491–519.

molecule, it is possible to influence the electron-transfer rates within the dyad, indicating a possible route to manipulate the rates to cause productive electron transfer to an electron relay.

Acknowledgment. We thank William W. Brennessel and the X-ray Crystallographic Facility of the Department of Chemistry at the University of Rochester. This work was supported by the U.S. Department of Energy, Division of Basic Sciences (DE-FG02-90ER14125).

Supporting Information Available: X-ray structure files (CIF), femtosecond TA spectra for complexes **1a**, **2**, **4**, and **7**, DFT optimized geometries, full TD-DFT excited state lists, frontier orbital diagrams, and complete ref 26. This material is available free of charge via the Internet at http://pubs.acs.org.

JA1070366